Chem Catalysis

CellPress

Review

The active phase in cobalt-based Fischer-Tropsch synthesis

Iris C. ten Have[1] and Bert M. Weckhuysen[1,*]

SUMMARY

Fischer-Tropsch synthesis (FTS) is an industrial catalytic process that converts a mixture of CO and hydrogen into long-chain hydrocarbons. These products are used as clean transportation fuels and chemical building blocks. The solid catalysts used in the process are complex multi-component systems. Therefore, unambiguously determining the catalytically active phase under reaction conditions remains challenging and thus a topic of debate. The active phase in cobalt-based FTS, including the reaction pathways it catalyzes, has been of industrial and academic interest for many years. It provides direct ways to control the output of the process. The delineation between an active and inactive phase is often unclear, as different phases (i.e., cobalt oxide, carbide, and metal) have different catalytic behavior. This review focuses on cobalt-based FTS materials, with a special focus on the industrially applied cobalt/TiO_2 system. The various cobalt phases are reviewed and discussed with respect to the most recent literature.

INTRODUCTION

Fischer-Tropsch synthesis (FTS) is a collective name for chemical reactions that convert a mixture of CO and hydrogen, coined synthesis gas or syngas, into long-chain hydrocarbons.[1,2] The most common overall reactions yield linear alkanes (Equation 1) or alkenes (Equation 2), although oxygenates such as alcohols can also be produced.[3]

$$nCO + (2n + 1)H_n \rightarrow C_nH_{2n+2} + nH_2O \quad \text{(Equation 1)}$$

$$nCO + (2n)H_2 \rightarrow C_nH_{2n+2} + nH_2O \quad \text{(Equation 2)}$$

This technology dates back to the 1920s[4,5] and initially coal was used as a feedstock to produce synthesis gas (Figure 1A). Later, natural gas and biomass were used, as synthesis gas can virtually be produced from any (hydro)carbon feedstock. In the light of climate change and sustainability, CO_2 seems an attractive renewable feedstock for future purposes.[6–8] Cobalt, iron, nickel, and ruthenium are all catalytically active in the FTS reaction. However, nickel is highly selective toward methane, while ruthenium is scarce and expensive. Generally, FTS is commercially conducted with cobalt- and iron-based heterogeneous catalysts. A conceptual representation of the FTS can be found in Figure 1B. Cobalt mainly yields linear paraffins and operates at 200°C–250°C. Iron, on the other hand, can operate in a wider temperature range (200°C–350°C) and generally produces more olefins and oxygenates, especially at the higher end of the temperature range (320°C–350°C).[1,2] Water and CO_2 are by-products of the FTS due to the water-gas shift (WGS) reaction (Equation 3):

$$CO + H_2O \leftrightarrow H_2 + CO_2 \quad \text{(Equation 3)}$$

Cobalt has a relatively low WGS activity[1] and is therefore more suitable for feedstocks with $H_2/CO \approx 2$, such as natural gas. Iron, on the other hand, possesses a

The bigger picture

Fischer-Tropsch synthesis offers an elegant solution to enrich energy supplies, mitigate CO_2 emissions, and minimize waste streams. This industrial catalytic process, which was invented almost a century ago, converts mixtures of H_2, CO, and CO_2 into clean transportation fuels and chemical building blocks. Understanding how the catalytically active phase arises and leads to the formation of a certain product is essential to maximize the catalyst performance. In this review, we present an overview of active and inactive phases in the cobalt-based Fischer-Tropsch synthesis and encourage the connection of fundamental insights with real industrial catalysis. Only then can we transition to a more circular and sustainable society.

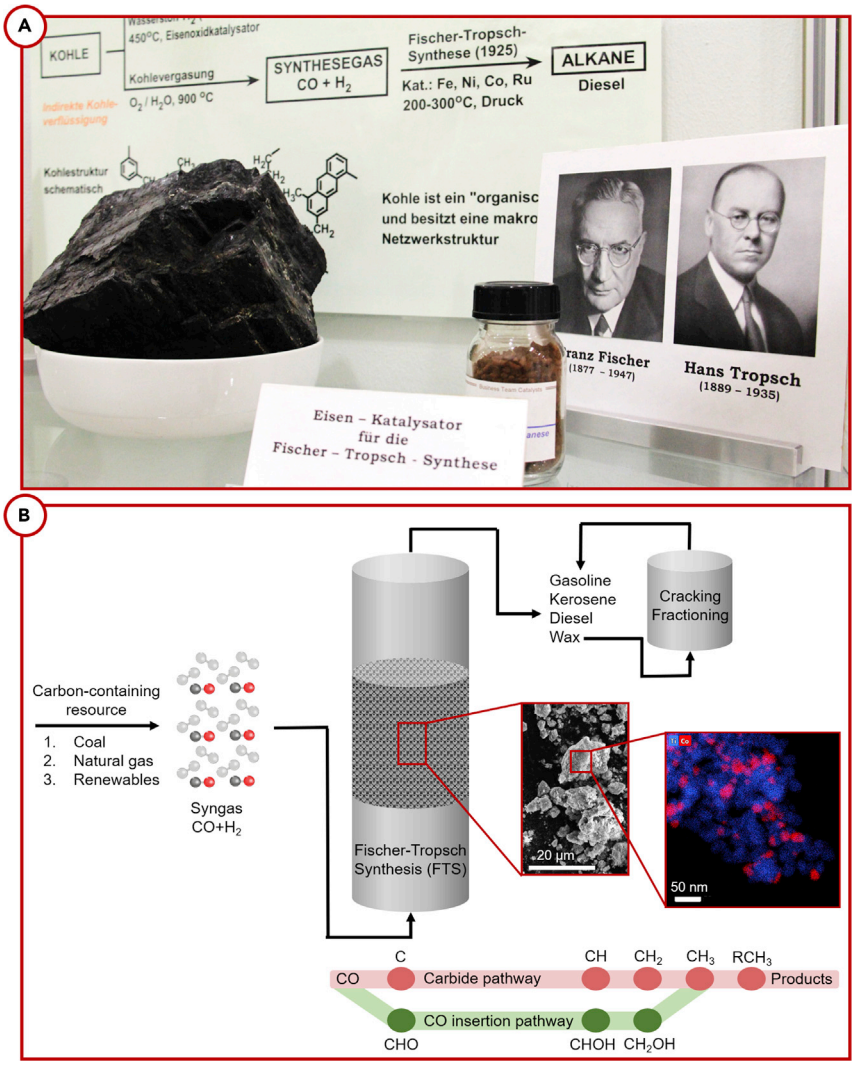

Figure 1. Overview of FTS

(A) Photograph taken at the Max-Plank-Institut für Kohlenforschung (Mülheim, Germany) displaying the first Eisen (iron) catalyst for FTS and the inventors Franz Fischer and Hans Tropsch.

(B) Conceptual overview of FTS: syngas, CO, and H_2 can be produced from virtually any carbon-containing resource. When FTS was invented in the 1920s, coal was used. Later, natural gas and nowadays more renewable resources, such as biomass, CO_2, and eventually perhaps municipal waste, can be used. The syngas is led over a solid heterogeneous catalyst material, containing iron or cobalt nanoparticles as the active component. The right side of (B) displays an electron microscopy image and X-ray elemental analysis of a typical FTS catalyst, cobalt nanoparticles (red) on a titania support (blue).

higher WGS activity and is often used for feedstocks with $H_2/CO \approx 1$, such as coal and biomass.[9] Maximizing the output of desired products remains an ongoing quest in heterogeneous catalysis research and there are many ways to do this; for example, by investigating catalyst deactivation,[1,10–14] reaction mechanisms,[15–20] and active phases.[10–13,21–24]

Catalyst deactivation is a major challenge in both cobalt- and iron-based FTS. The large industrial and academic interests in this subject are not surprising. Replacing a catalyst regularly is very unfavorable from a commercial point of view, and

[1]Inorganic Chemistry and Catalysis Group, Debye Institute for Nanomaterials Science, Utrecht University, Universiteitsweg 99, 3584 CG Utrecht, the Netherlands

*Correspondence: b.m.weckhuysen@uu.nl

https://doi.org/10.1016/j.checat.2021.05.011

understanding the pathways responsible for the complex deactivation behavior of catalytic systems is interesting from an academic perspective. Even though significant research efforts have been made over the past years,[1,9–13] deactivation remains a topic of debate in the open literature.[1] Many different processes are at interplay simultaneously, of which sintering,[25,26] re-oxidation,[1,21] metal-support reactions,[21,26,27] and carbon deposition[12] are just a few examples.

Understanding which reaction mechanisms are responsible for the formation of certain products is another way to maximize the desired output. For the FTS, the C–O bond scission and C–C coupling mechanisms are particularly interesting. Promoting these pathways would enhance the activity and selectivity during the reaction. Various mechanisms have been proposed for CO dissociation and chain growth. Although not unquestioned, direct dissociation of CO followed by carbon hydrogenation and polymerization of CH_x is advocated by most researchers.[15–18] The most widely accepted alternative is the H-assisted C–O scission and chain growth by CO insertion.[15,16,19,20] Reaction mechanisms remain a controversial topic, as conclusive experimental evidence is rather scarce. The FTS reaction mechanisms will be summarized in the section reaction mechanisms in FTS.

Identifying the active phase(s) in the catalyst under reaction conditions is a promising approach to maximize the FTS product yield. FTS catalysts typically consist of metal oxide nanoparticles before the reaction; i.e., Co_3O_4 in the case of cobalt and Fe_2O_3 in the case of iron. To convert the catalyst to the active form, it is treated with H_2, or potentially CO/synthesis gas for iron. In general, it is recognized that metallic and oxidic species coexist after activation and during FTS. For iron, carbidic species may exist if the catalyst was activated in CO/synthesis gas, which are believed to be the active phase in iron-based FTS. For cobalt, on the other hand, the metallic form is considered the active phase. This difference (i.e., carbide versus metal) is quite remarkable and underlines the complexity of identifying the active phase(s), as the two metals catalyze an almost identical chemical process with presumably comparable reaction mechanisms.

The recent shift toward a more sustainable and circular society has revived interest in FTS catalysts, since CO_2 could be used as feedstock for synthesis gas or perhaps even as reactant directly. This review focuses on cobalt-based FTS catalysts, with cobalt/TiO_2 in the spotlight. We will present different viewpoints throughout history on the origin of catalyst (de)activation and discuss experimental evidence confirming or opposing these viewpoints (sections origin of cobalt and cobalt phases in FTS and the history of the disputed active phases in cobalt FTS). Then, an overview of the active/deactivating phases found during FTS will be discussed thoroughly in section discussion of the different hypotheses on the cobalt active phase, followed by a more detailed debate on the cobalt/TiO_2 system including promising characterization techniques in section the cobalt/TiO_2 showcase. Special attention will be given to the role of carbon in catalyst (de)activation.

REACTION MECHANISMS IN FTS

The FTS reaction mechanism has been a topic of debate ever since the first papers were published by Fischer and Tropsch[4,5] (Figure 1A). The development of surface science tools,[15,20,28–34] as well as *in situ* and *operando* studies,[10,11,13–15,35,36] has significantly increased our understanding. Nevertheless, the dispute around reaction mechanisms in FTS is still ongoing. As an in-depth mechanistic discussion would be beyond the scope of this review, we will only provide a brief overview of the three

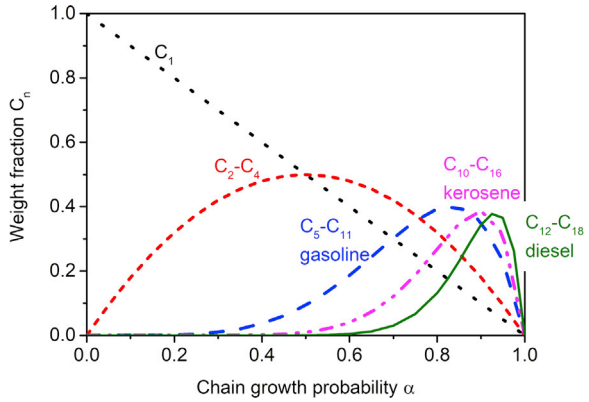

Figure 2. Hydrocarbon product distribution
Weight fraction Cn with chain length n plotted as a function of the chain growth probability factor α.

main mechanisms that have been proposed. Generally, all the relevant mechanisms can be divided into three elementary steps[37]:

1. Chain initiation
2. Chain growth
3. Chain termination

These steps are accurately described by the Anderson-Schulz-Flory (ASF) model.[38,39] This model presumes the FTS reaction as an ideal polymerization reaction with a single chain growth probability factor α, which determines the hydrocarbon chain length n (Figure 2). The optimal value for α depends on the application. For small chemical building blocks, like ethylene and propylene, a low α value is desirable, whereas, for longer molecules, for example transportation fuels such as C_{12}–C_{18} diesel, a higher value is required (Figure 2). The three main reaction mechanisms proposed for FTS are described below and depicted in Figure 3.

Carbide mechanism

The first[4,5] and most widely accepted mechanism[15–18,40] in cobalt-based FTS is the carbide mechanism. This mechanism presumes direct dissociation of CO and H_2, followed by hydrogenation of carbon atoms, and polymerization of CH_x. Chain termination takes place either by abstraction or addition of a hydrogen atom from or to the chain.

CO insertion mechanism

The second mechanism proposes the adsorption of CO, followed by a reaction with hydrogen atoms on the surface to an aldehyde functionality (COH).[15,16,19,20] Chain growth takes place by insertion of CO and chain termination by hydrogenation. For flat cobalt terrace sites, it has been established that this mechanism has a lower energy barrier than the direct dissociation of CO.[16,19,20,40] It is therefore not unthinkable that multiple reaction mechanisms occur simultaneously during the FTS.[41]

Hydroxycarbene mechanism

A third mechanism proposes the adsorption of CO, followed by a reaction with hydrogen atoms on the surface to a hydroxycarbene group (CHOH).[17,37] Chain growth of these species can take place by condensation polymerization, losing H_2O, or the individual hydroxycarbenes can first be hydrogenated and then undergo condensation polymerization. Chain termination occurs via hydrogenation. For this

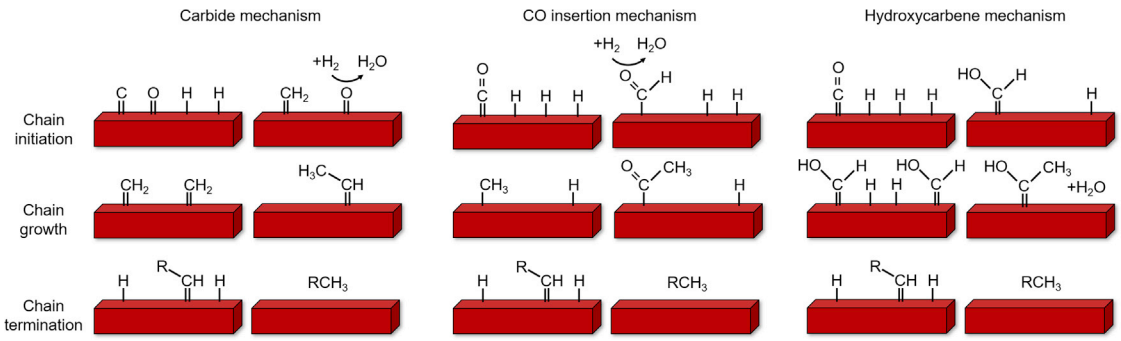

Figure 3. Schematic of the three main mechanisms in FTS

Representations of the carbide, CO insertion, and hydroxycarbene mechanism. The three elementary steps of chain initiation, growth, and termination are depicted from top to bottom.

mechanism there are, however, no strong experimental indications on realistic FTS catalysts.[17]

Apart from the reaction mechanism, the rate-determining step is also still under debate. CO dissociation,[42,43] carbon hydrogenation,[42,44] oxygen removal,[17,42,45] and chain termination[17,44,46] have all been mentioned before as rate-controlling steps. Reaching a consensus on this is difficult, as parameters like temperature and hydrogen availability influence the rate-determining step too.[17] It has, for example, been reported that CO dissociation is the dominant rate-controlling step at low temperatures, while hydrogenation becomes more rate controlling at higher temperatures.[47] Besides, the cobalt phases present under reaction conditions are of paramount importance for the resulting activity and selectivity.

ORIGIN OF COBALT AND COBALT PHASES IN FTS

Cobalt occurs naturally in the Earth's crust in the form of ores, chemically combined with other elements. The name cobalt is derived from the German word kobold, which means goblin or evil spirit.[48,49] This refers to the challenging mining process, in which arsenic and sulfur fumes were released while isolating cobalt from the ores. Besides, cobalt occurs naturally as an organometallic complex in vitamin B_{12}, which is produced by microbes in soil and the marine environment.[50] Today, cobalt has applications in, for example, the paint industry, lithium-ion batteries, gas sensors, and catalysis.[49] Cobalt-based FTS catalysts are typically synthesized from a metal salt precursor and the fresh cobalt catalyst, containing cobalt oxides (Figure 4), is obtained by applying a calcination procedure. The catalyst is then activated in H_2 at elevated temperatures, as metallic cobalt is generally postulated as the active phase.[2,21] However, metallic cobalt is most often not the only phase present under reaction conditions (Figure 4) and it has been mentioned before that cobalt oxides,[22,37,51] cobalt carbide,[11,52–54] cobalt with carbon deposition,[10,31] and cobalt-support interfaces[22,35,51] are catalytically active as well. The debate around the cobalt active phase in FTS dates back to the 1920s and in the next section we will elaborate on the history of this disputed active phase.

THE HISTORY OF THE DISPUTED ACTIVE PHASES IN COBALT FTS

In 1902, Sabatier and Senderens[55] first published results of synthesis gas conversion into methane over nickel and cobalt catalysts. In the 1920s, Fischer and Tropsch[4,5] found out that synthesis gas could also be converted into long-chain hydrocarbons, which could be used as fuel. In their first patent in 1925, they described the use of cobalt- and iron-based catalysts at atmospheric pressure below 300°C.[56] Different

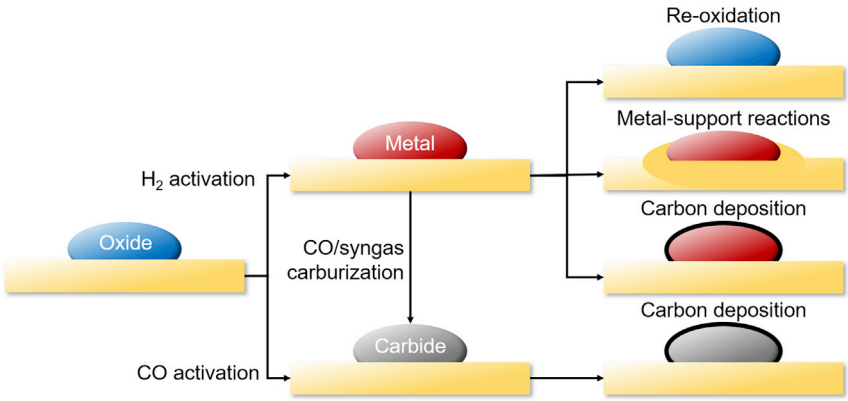

Figure 4. Schematic of various proposed (in)active phases in FTS

The fresh catalyst typically consists of supported metal oxide nanoparticles (left). After activation in H_2 or CO, the catalyst contains a metal or carbide, respectively (middle). Besides, the metallic catalyst can be converted to a carbide with CO or syngas. Re-oxidation, metal-support reactions, and carbon deposition may occur under reaction conditions (right).

claims have been made over the past century regarding the (de)active phase(s) and (in)active sites in cobalt-based FTS catalysts. A chronological overview of these claims is presented in Figure 5.

In 1930, Fischer and Tropsch[57] specifically mentioned the "metallic catalyzer" cobalt as an active component in their patent. However, multiple studies from 1931 to 1945[58–61] described cobalt carbide as an "unstable intermediate" in the FTS reaction. For example, Herington and Woodward[60] proposed in 1939 that cobalt carbide was responsible for the formation of CH_2 groups and polymerization into long-chain hydrocarbons, while metallic cobalt was considered responsible for chain termination by hydrogenation. Hofer and Peebles[62] reported in 1947 using X-ray diffraction (XRD) that face-centered cubic (FCC) cobalt is formed upon reduction of cobalt/SiO_2 in H_2 at 400°C. They then carburized the catalyst to cobalt carbide and reduced it again, which led to the formation of the more active hexagonal closest packed (HCP) cobalt.[62]

The hypothesis that cobalt carbide was an active intermediate in the FTS reaction was invalidated by Weller et al. using XRD in 1948.[63] In the same year, Kummer et al.[64] showed with ^{14}C as a tracer that only 10% of the hydrocarbon products were formed via a surface cobalt carbide. Carbon deposition and cobalt carbide formation were mentioned as deactivation mechanisms in the cobalt-based FTS reaction in a patent by Mattox in 1950.[65] Cobalt carbide was still disregarded as a plausible intermediate in the FTS in 1959 and studies became increasingly focused on the FTS reaction mechanism.[66] However, in the 1960s, the interest in FTS decreased due to the large availability of crude oil.

In the 1970s and 1980s, the interest in FTS was renewed due to oil crises and the sanctions toward South Africa.[2,9] In this era, many studies were focused on unraveling the complicated and multifaceted FTS reaction mechanisms.[67] In 1984, Reuel and Bartholomew[68] published a comprehensive study on support and dispersion effects in the cobalt-based FTS. They mentioned, among other things, that an increasing "extent of reduction", i.e., metallic cobalt, had a positive influence on the activity and selectivity toward long-chain hydrocarbons.[68,69] This claim was substantiated during the 1990s by multiple studies using catalytic testing, temperature

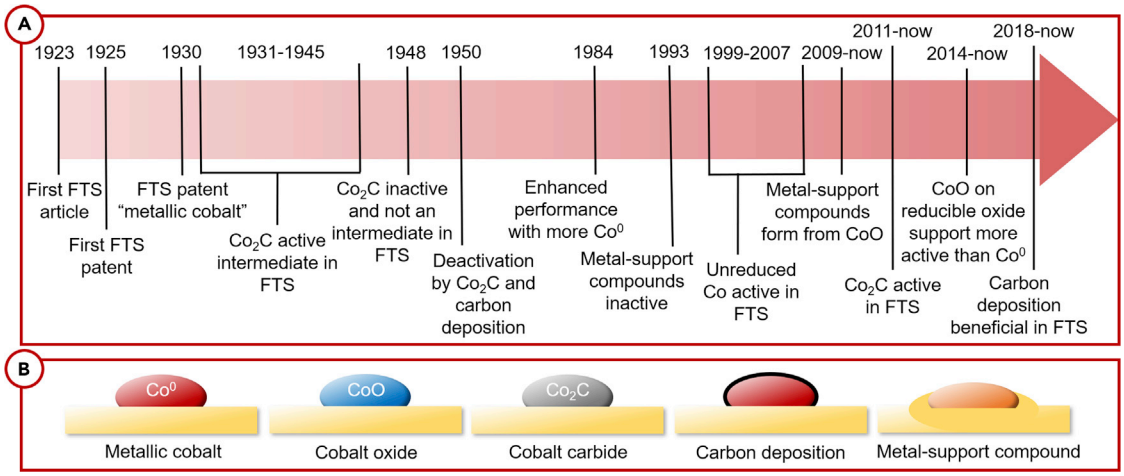

Figure 5. Chronological overview of the proposed (in)active phases in the cobalt-based FTS

(A) Varying claims have been made throughout the almost 100 years of FTS history.

(B) Schematic overview of the different (in)active cobalt phases.

programmed reduction (TPR),[70–72] and X-ray photoelectron spectroscopy (XPS).[73] These studies also postulated that metal-support compounds, such as cobalt aluminates and cobalt silicates, were inactive in the FTS reaction.[70–73] The development of *in situ* characterization methods, such as infrared (IR) spectroscopy and XRD, contributed to the finding that not only metallic cobalt was capable of adsorbing CO; cobalt oxide could do that as well.[74] These developments also brought to light that metallic cobalt and cobalt oxides almost always coexist under FTS reaction conditions.[74] In 1999, Ernst et al.[75] concluded that a higher percentage of unreduced cobalt did not necessarily influence the activity, but shifted the selectivity from C_{22+} (waxes) to C_5–C_{13} (gasoline). This suggests that cobalt oxides are active in the FTS reaction as well. Interestingly, many important hypotheses around the active phase in cobalt-based FTS had already been formed during the first 75 years after the invention of FTS. However, the instrumentation required to prove or disprove these hypotheses had not yet fully been developed. The beginning of the 21st century marked a new and fruitful era for methodology development. For example, various surface science tools as well as *in situ* and *operando* studies have contributed to our increased understanding of the active phase in FTS.

In the 2000s, the FTS process was revived even more due to resource depletion and environmental concerns.[76] Many investigations were focused on the effect of cobalt nanoparticle size and it was found that smaller nanoparticles ($\leq$6 nm) are more difficult to reduce than larger ones.[77–80] From 2004 to 2007, Morales, Weckhuysen, and coworkers published multiple papers on the TiO_2 support and MnO promoter effects in cobalt FTS.[81–87] One of the findings they reported was that MnO decreased the reducibility of cobalt, but enhanced both the FTS activity and selectivity toward C_{5+} hydrocarbons.[81,83] This suggested again that cobalt oxides could be active in the FTS. However, it was also found that cobalt oxides resulting from re-oxidation by water could form inactive metal-support compounds more easily than metallic cobalt.[1,21,76] For metallic cobalt, it had already been established that the HCP crystal phase was more active in FTS than the FCC crystal phase.[62,76] Saib et al.[88] reported for metallic cobalt the B_5 step-edge sites as the most active sites in FTS. These B_5 sites were first introduced in the 1960s to describe the crystallite size effect on N_2 adsorption,[89,90] but they were not specifically linked to cobalt-based FTS until 2010.[88]

From 2011 until now, multiple studies have appeared reporting cobalt carbide as a highly active phase in the cobalt-based FTS toward olefins[52,91–93] or oxygenates.[53,91,94–97] All these studies mentioned that cobalt carbide was stabilized by and in synergy with an oxidic compound and/or an alkali promoter. Until now, cobalt carbide has also been reported as deactivating by studies that did not use oxidic compounds or alkali promoters.[1,11,13,98–100]

From 2014 until now, evidence has been presented that cobalt oxide supported on TiO_2 was more active in both FTS and CO_2 hydrogenation than its metallic cobalt variant.[22,101] Similarly for cobalt/Al_2O_3, an increased CO_2 hydrogenation to ethanol activity has been reported due to coexisting cobalt and cobalt oxide phases.[102] For MnO_x/Co_3O_4 as well; the cobalt oxide phase has been reported more active than metallic cobalt in the CO_2 hydrogenation toward methanol.[51] However, for cobalt/SiO_2 the opposite has been reported: the metallic variant was more active.[22] The presence of a (somewhat) reducible oxide thus seems vital for enhancing the FTS performance of cobalt oxides.

In 2018, two studies emerged reporting that carbon deposition was beneficial for generating an active FTS catalyst.[10,103] It was also reported that graphitic carbon species could particularly block methanation sites[103] and that a higher cobalt valence state could be correlated to the degree of saturation in the carbon deposits.[10] Research on this topic is still ongoing and the development of, among other things, surface science tools is vital for our understanding.

DISCUSSION OF THE DIFFERENT HYPOTHESES ON THE COBALT ACTIVE PHASE

General properties of metallic cobalt and its role in FTS

Metallic cobalt is a solid with a silvery blue color and magnetic properties.[48,49] Metallic cobalt can exist in three different crystal phases: HCP (lattice parameter a = 2.507 Å[104]), FCC (a = 3.538 Å[105,106]), or cubic primitive (CP).[37] Under FTS reaction conditions, the HCP and FCC crystal phases are the main allotropes reported for cobalt nanoparticles (Figure 6).[35]

In bulk cobalt, the transition from FCC to HCP occurs around 400°C,[37] but can occur at temperatures $\leq$300°C for metal nanoparticles.[107] HCP cobalt nanoparticles have been reported to have a higher FTS activity compared with FCC cobalt.[43,76,108] Theoretical results indicated a higher CO dissociation rate on most HCP facets than on FCC facets and thus a higher intrinsic FTS activity on HCP cobalt.[109] Besides, theoretical calculations suggested that direct dissociation of CO is more favorable on HCP cobalt, while hydrogen-assisted CO dissociation is preferred on FCC cobalt. The higher intrinsic activity of HCP cobalt is related to the higher surface energy compared with FCC cobalt, caused by the lower coordination numbers of the surface atoms. Although this property may be beneficial for activity, it has a negative influence on the stability of the metallic cobalt phase under reaction conditions. HCP cobalt has been reported less resistant to water-induced re-oxidation[21] and to cobalt carbide[11] formation.

The size of the cobalt nanoparticles has an influence on the crystal phase and on the available surface sites under reaction conditions. It was found that as-synthesized cobalt nanoparticles $\leq$20 nm are pure FCC phase, ~30 nm a mixture of FCC and HCP, and $\geq$40 nm almost pure HCP.[107] For the FTS reaction, the optimum cobalt nanoparticle size is established at 6–8 nm (Figure 7A).[110,111] For such a catalyst, one would thus expect the pure FCC phase. In practice, however, a (partial) phase

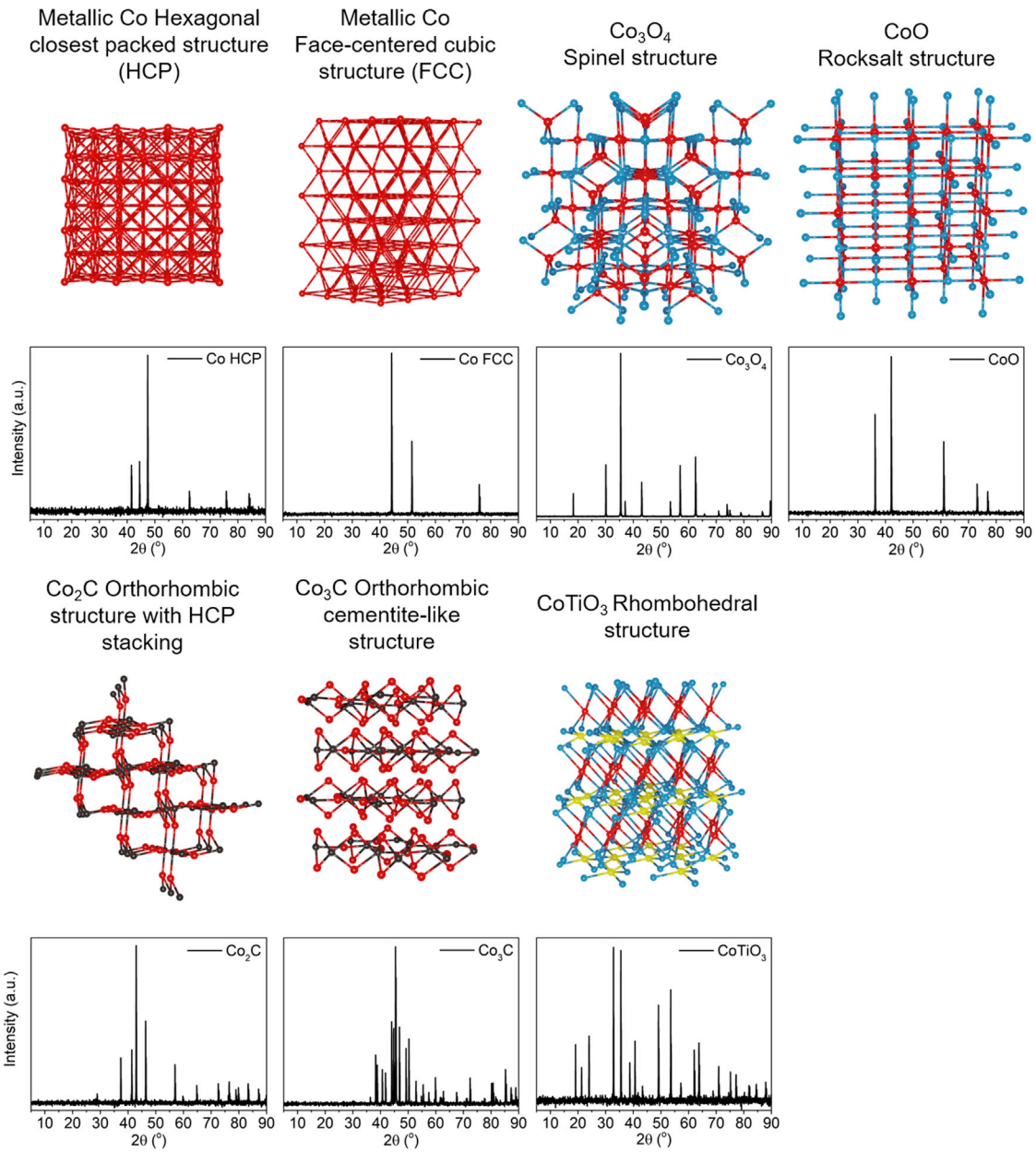

Figure 6. Relevant cobalt crystal structures in FTS

Crystal structures (top row from left to right) of HCP metallic cobalt, FCC metallic cobalt, $Co_3O_4$with spinel structure, cobalt oxide with rock salt structure (third row from left to right), Co_2C with orthorhombic structure and HCP stacking, Co_3C with orthorhombic cementite-like structure, and $CoTiO_3$ with rhombohedral structure (representing metal-support compounds). The second and fourth rows display simulated XRD patterns (Cu Kα radiation) for each structure.

transition to HCP may take place during the activation procedure and under FTS reaction conditions.[11] Below this optimum size, the catalyst produces more undesired methane and is more prone to re-oxidation.[21] Above this size, the turnover frequency is lower. This is related to the available surface sites. For small nanoparticles, the lower reactivity toward FTS is often ascribed to the lack of reactive B_5 step-edge sites.[112] The term "B_n site" was first used by van Hardeveld and Hartog[89] in the 1960s to indicate an ensemble of n surface atoms that are in close contact with an adsorbed species to the site (Figure 7B).

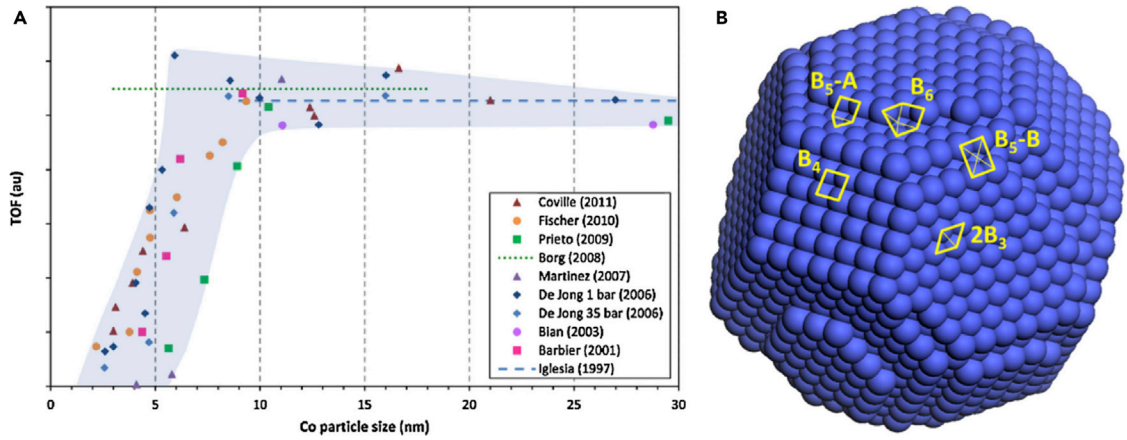

Figure 7. The cobalt particle size effect in FTS

(A) Size-dependent turnover frequency (TOF) in FTS as a function of the cobalt nanoparticle size. Reproduced from van de Loosdrecht et al.[2] and van Helden et al.[105] and elsewhere.[110,111,113–117]

(B) A 4-nm metallic cobalt nanoparticle (FCC) showing different Bn sites, including two types of reactive B5 sites. Reproduced from van Helden et al.[105]

General properties of cobalt oxides and their role in FTS

Cobalt oxides are generally crystalline solids with a dark color. While three different cobalt oxides exist, only Co_3O_4 and cobalt oxide have been well characterized and are of potential importance in the FTS reaction. Cobalt (III) oxide, Co_2O_3, is a dark gray to black crystalline powder. The compound has been reported as metastable with a hexagonal HCP structure in the literature.[118] Co_2O_3 is not as well characterized as other cobalt oxides; it is still uncertain whether or not it can exist as a stable solid crystal. Cobalt (II,III) oxide, Co_3O_4, is a black antiferromagnetic solid and one of the two well-characterized cobalt oxides.[118] It has applications in, for example, lithium-ion batteries, gas sensors, electrochemistry, and catalysis. Co_3O_4 has a normal cubic spinel structure (a = 8.020 Å[118]), as depicted in Figure 6, and is the thermodynamically favored cobalt oxide under ambient conditions. Cobalt (II) oxide, referred to here as cobalt oxide, is an olive green or gray solid with applications as a coloring agent in the ceramics industry, electrochemistry, and catalysis. It has a rock salt crystal structure (a = 4.258 Å[118]) consisting of two interpenetrating FCC sublattices of Co^{2+} and O^{2-} (Figure 6).[118]

Typically, the fresh FTS catalyst material containing Co_3O_4 is activated at elevated temperatures in H_2 via cobalt oxide to metallic cobalt. However, it is generally accepted that cobalt oxide and metallic cobalt coexist under FTS reaction conditions.[10,35,119–121] Small metallic cobalt nanoparticles can easily re-oxidize to cobalt oxide/Co_3O_4 during FTS due to the production of water,[21,122,123] which has been considered as a deactivation mechanism.[124] Additionally, it has been reported that cobalt oxide is thermodynamically more likely than metallic cobalt to undergo metal-support solid state reactions and form inactive metal-support compounds,[21] such as cobalt titanates ($CoTiO_3$, a = 5.485 Å[125]) or cobalt aluminates ($CoAl_2O_4$, a = 8.105 Å).[121,126] There is a discrepancy between different studies regarding the role of cobalt oxides in FTS. To clarify this, we should take into account the cobalt nanoparticle size, support material, and reaction conditions.

Some studies report irreducibility and/or re-oxidation of 2–3 nm cobalt metal nanoparticles,[126] whereas others mention a re-oxidation threshold of 5.3 nm[121] or 7.5 nm.[122] A safe lower size limit would thus be ~8 nm to control and, if desired, avoid re-oxidation.

The support material seems to have a major influence on the performance of cobalt oxides in the FTS and CO_2 hydrogenation reaction. Evidence has been presented that cobalt oxide supported on TiO_2 was more active in both FTS and CO_2 hydrogenation than its metallic cobalt variant.[22,101] However, in the same study it was mentioned that, on SiO_2 support, metallic cobalt was more active. This effect was ascribed to a unique interface between cobalt oxide and the reducible TiO_2 support.[22] In another study, it was found that cobalt/Al_2O_3 converted CO_2 into ethanol with high selectivity due to coexisting cobalt and cobalt oxide phases.[102] However, specific active sites for cobalt oxides have to our best knowledge not yet been reported in the open literature. However, intuitively, one could imagine that a stepped rather than a flat surface composes the active sites, as both FTS and CO_2 hydrogenation are structure-sensitive reactions.[127] For example, for cobalt oxide with rock salt structure, a plausible active site in terms of B_n site could be B_5O_2, where B represents cobalt atoms, O represents oxygen atoms, and n denotes the number of atoms in close contact to an adsorbed species.

Reaction conditions are of paramount importance to the cobalt and/or support phases present in the catalyst. At high conversion rates, when the water production is high, cobalt and/or cobalt oxide may more readily form inactive metal-support compounds.[21] Also, the reaction temperature cannot be overlooked. While deactivating cobalt aluminates have been reported at high conversion rates and reaction temperature 220°C–250°C,[121,122,126] coexisting cobalt and cobalt oxide on Al_2O_3 support were mentioned as active phase at 140°C–200°C.[102]

While metallic cobalt is generally accepted as active phase, cobalt oxides coexist under FTS reaction conditions. Cobalt oxides can be (part of) the active phase, provided that the support material is not SiO_2 and that they do not form inactive metal-support compounds. Besides, it is important to mindfully design the catalyst synthesis procedure and to choose suitable reaction conditions.

General properties of cobalt carbide and its role in FTS

Cobalt carbide is currently known to exist as cobalt carbide and Co_3C (Figure 6). Cobalt carbide, is a gray/black paramagnetic solid with noble metal-like properties[95] and an orthorhombic crystal structure (a = 2.877 Å[98]), isomorphous to η-Fe_2C. η-Fe_2C is a carbon-rich iron carbide that is unstable under FTS reaction conditions without the presence of an alkali promoter.[23] It is thus likely that cobalt carbide needs to be stabilized by alkali metals too. Co_3C has an orthorhombic crystal structure as well (a = 4.483 Å[128]), but has been characterized to a lesser extent than cobalt carbide. However, Co_3C has been mentioned before as isomorphous to θ-Fe_3C (cementite).[128,129] The carbon-poor θ-Fe_3C has been associated with deposition of deactivating carbon species on the catalyst surface and the carbide phase is not necessarily stabilized by alkali promoters.[23] In iron-based FTS, χ-Fe_5C_2 (Hägg carbide) has been postulated as the most stable active phase under reaction conditions. However, such an isomorph has not been mentioned before in cobalt-based FTS. Besides in catalysis, carbides have found applications in cutting tools, machinery, and ammunition for their hardness and mechanical strength.

While iron carbides are considered as active phase in FTS,[23,24] the formation of cobalt carbides and their role in the FTS reaction is a controversial topic. Carbon diffusion in iron (43.9–69.0 kJ/mol) occurs more easily than in cobalt (145 kJ/mol),[130,131] but the two metals have quite similar activation energies for the FTS reaction, 89.1 and 105 kJ/mol respectively.[132] Because of this, iron catalysts first go through an initiation period in which carbides, are formed and at least six different types of

carbides have been reported in iron-based FTS.[9] On the other hand, CO and H_2 are readily converted into FTS products over cobalt catalysts. Cobalt carbides can, however, be formed under FTS conditions, particularly at low H_2/CO ratios.[11,99] Although only cobalt carbide and Co_3C have been reported thus far, more cobalt carbide polymorphs may exist. The formation of cobalt carbides is exothermic and they are less stable compared with iron carbides.[99,133] An underlying reason for their instability is the geometry of the crystal phase. The unit cells of hexagonal facets in HCP cobalt match well with hexagonal graphitic structures, whereas the predominantly body-centered cubic (BCC) iron facets do not present a good match for graphite.[133] Therefore, the formation of graphitic carbon on cobalt may be more favorable than the formation of cobalt carbides.[11,99]

Some studies correlate cobalt carbide formation to higher selectivity toward lower olefins[52,91–93,134–136] or oxygenates,[53,91,94–97,135,137,138] while others relate it to catalyst deactivation.[1,11,13,98–100] The role of cobalt carbides in the FTS reaction is thus rather ambiguous and evokes further discussion. We should remind ourselves that cobalt-based FTS catalysts do not only contain cobalt but also a support material and often promoter elements. Interestingly, most studies that report an increased olefin or oxygenate selectivity upon cobalt carbide formation use catalysts containing an oxidic compound, like MnO[52,91–93,96,135,139–142] or La_2O_3,[94,143] and/or an alkali promoter.[53,91,134] For iron-based catalysts, it is well established that the alkali promoters sodium[23,24] and potassium[144,145] act as structural stabilizers for iron carbide formation. As cobalt carbides are intrinsically less stable than iron carbides,[146] the presence of an alkali metal may even be more essential for stabilization of the cobalt carbide phase. Besides, synergistic effects at the interface of cobalt carbide and the oxidic compound, MnO or La_2O_3, seem to be responsible for the enhanced selectivity toward olefins or oxygenates.[91]

Similar to metallic cobalt, particle size effects were reported for cobalt carbides as well. The optimum cobalt carbide nanoparticle size was established at ~7 nm.[147] Below that size, the turnover frequency was lower and the methane selectivity was higher. Above that size, the turnover frequency decreased again. The particle size effects for cobalt carbides were, as for metallic cobalt, linked to the available surface sites.[97,141,147,148] Small nanoparticles mainly exposed the $Co_2C(111)$ surface, which favored methane formation.[147,148] The stepped $Co_2C(101)$ and $Co_2C(020)$ surfaces were responsible for olefin formation.[147] We would herein like to conform the active sites on cobalt carbide nanoparticles to the B_n site notation. B then represents cobalt atoms, C represents carbon atoms, and n denotes the number of atoms in close contact to an absorbed active species. The $Co_2C(101)$ surface is then noted as B_9C_2 and the Co_2C (020) surface as B_6C_1.

Even though metallic cobalt is generally accepted as the active phase, cobalt carbides may represent a hidden gem in FTS catalysis, provided that the cobalt carbide phase synergizes with an oxidic compound and/or an alkali promoter.

General properties of carbon deposition and its role in FTS

Carbon deposits are generally gray or black solid films that can either be crystalline or amorphous, depending on their structure. The most well-known crystalline carbon allotropes are diamond, with a cubic crystal structure, and graphite, with a hexagonal crystal structure. Diamond is applied in, for example, cutting tools and gemstones. Graphite is used in pencils and lubricants, as well as electronics for its high conductivity. Only graphite is formed as crystalline carbon deposition on catalyst surfaces.

Amorphous carbon could be any kind of carbon allotrope without crystalline structure. The properties of amorphous carbon are dependent on sp2 and sp3 ratios and can vary strongly. These types of carbon are, for example, applied as pigments, gas storage materials, or in catalysis.[149]

Similarly to cobalt carbides, the role of carbon deposits in cobalt-based FTS remains rather obscure. Some studies describe carbon deposition as deactivation mechanism,[12] while others argue that carbon deposition is beneficial for generating an active FTS catalyst.[10,103] To offer some clarification, we should first divide carbon deposits into atomic, amorphous aliphatic, amorphous (poly)aromatic, crystalline, and subsurface. Atomic carbon is a single carbon atom on the cobalt surface resulting from C–O bond scission. These carbon atoms are considered the most reactive type of carbon deposition.[31] Amorphous carbon is a relatively reactive type of carbon deposition and can often be removed from the cobalt surface by hydrogenation.[103] Crystalline carbon represents a class of carbon materials with a highly ordered structure. Graphite, a monolayer of sp2 carbon atoms arranged in a hexagonal lattice, is the most relevant type of crystalline carbon in the FTS reaction. Multiple layers of graphite stacked on top of each other is referred to as graphene. Subsurface carbon describes carbon atoms at interstitial positions of a metal lattice.[106]

Atomic carbon has been reported to weaken the adsorption of CO and H_2.[31] However, it is also an intermediate in the FTS reaction and does not prevent the cobalt surface from adsorbing reactants. Therefore, atomic carbon is not considered a detrimental form of carbon deposition.

Amorphous aliphatic carbon deposits are relatively reactive and can easily be removed from the surface by hydrogenation at typical FTS reaction temperatures <260°C.[12,103] Such deposits, for example, a growing hydrocarbon chain, are generally intermediates in the FTS reaction and not considered detrimental to catalyst performance.

Amorphous (poly)aromatic carbon deposits are typically less reactive than the aliphatic version. It is known that (oxygenated) (poly)aromatic (hydro)carbon deposits form on cobalt-based catalysts during the FTS reaction.[10,103] These species are only considered detrimental if they cannot be removed from the surface by hydrogenation below 350°C.[12,28]

Crystalline (graphitic) carbon can arise from amorphous carbon structures on the catalyst surface and is known to kinetically, thermodynamically, and geometrically prefer flat cobalt terrace sites over step edges.[103] When such species are irreversibly adsorbed on the catalyst surface, they are considered as deactivating. However, graphitic carbon has also been reported to selectively block methanation sites.[103] This could be interesting for FTS, as methane is an unwanted side product.

Subsurface carbon arises from diffusion of atomic carbon on the catalyst surface into the metal lattice. Some studies mentioned that subsurface carbon may decrease catalyst activity.[1,12] However, it has been reported before that carbon migration to subsurface cobalt layers is only energetically feasible at high carbon coverage and unlikely to occur to a significant extent under FTS conditions.[106] Subsurface carbon may precede and initiate the formation of bulk cobalt carbides.[140] Similarly to cobalt carbides, subsurface carbon may thus require the presence of oxidic surfaces and/or alkali promoters to be stabilized.

Carbon deposition is a rather broad collective term that can be confusing when not elaborated. It essentially describes all carbon on the catalyst surface, ranging from a single carbon atom to vast sheets of graphitic carbon. Some of them are intermediates in the FTS reaction, while others block certain active sites. Hence, it is indispensable to clarify the specific structure when describing carbon deposits, as they can either be advantageous or detrimental. When used sensibly, carbon deposition is a promising tool for tweaking selectivity in the FTS reaction.

General properties of cobalt-support interfaces and their role in FTS

Transition metals, like cobalt, are known to interact with metal oxide supports and the strength of these metal-support interactions (MSIs) correlates with the reducibility of the support. The strong metal-support interactions (SMSIs) between transition metals and the reducible TiO_2 support, leading to reduced CO and H_2 chemisorption, were first described by Tauster et al.[150] in 1978. They explained that Ti^{4+} can be reduced to Ti^{3+}, which then transfers an electron to the supported metal atom. This would result in a strong ionic bond between Ti^{3+} and the metal.[151,152]

Support materials used in heterogeneous catalysis are typically not inert and their interactions with metal nanoparticles may give rise to interfaces with special properties. Such interfaces have been reported to enhance catalytic performance in the cobalt-based FTS and CO_2 hydrogenation.[152–155] Over the past few decades, varying reasons for this behavior have been mentioned in the literature. Understanding these special interfaces is of great significance in rational catalyst design.

The two main factors contributing to MSIs are electronic and geometric. The electronic factor results from charge transfer between the support and the metal, while the geometric factor originates from a thin layer of reduced support oxide covering the metal.[156] The strength of MSIs depends on the reducibility of the support oxide. If MSIs are too strong, they are considered deleterious for catalyst performance,[157] in particular, when support oxide patches are covering active sites or when solid state reactions form an inactive metal-support compound.[21,121,126] However, when MSIs are too weak, they will not influence the catalytic performance at all and, in order to benefit from MSIs, it is thus essential to find the optimum interaction strength.

Theoretical and experimental evidence suggests that the interface between cobalt and reducible oxides, like TiO_2,[22,155] CeO_2,[96,153] La_2O_3,[94] or MnO,[51,86,87] offers a low-energy reaction pathway and thereby enhances FTS and CO_2 hydrogenation activity. Various elemental steps have been mentioned to occur via these low-energy reaction pathways at cobalt-support interfaces. For FTS catalysts, CO dissociation[158,159] as well as C–C coupling[160] have been postulated as the facilitated elementary steps at the metal-support interface. More specifically for cobalt FTS catalysts, CO and CO_2 dissociation have been mentioned for Co–TiO_2,[22,155] possibly due to electron transfer from Ti to cobalt. For Co–CeO_2, CO and CO_2 dissociation were the facilitated elementary steps as well, potentially due to the formation of oxygen vacancies in the CeO_2 support.[96,153]

La_2O_3 and MnO are mostly used as promoters rather than support materials. However, they are widely used in FTS, so we will briefly discuss them here. Like the previously mentioned reducible oxides, La_2O_3[161] and MnO[87] facilitate electron transfer. However, instead of donating electrons, they both withdraw electrons from cobalt and decease the reducibility. For Co–La_2O_3, theoretical evidence pointed to C–C coupling as the elemental step to occur via a low-energy reaction pathway.[94] This enhanced the selectivity to higher alcohols. With MnO, the lower reducibility of

cobalt resulted in lower hydrogenation activity and less of the unwanted product methane.[85,87] Besides, MnO increases olefin/paraffin ratio and oxygenates,[85,162] likely due to its activity in the WGS reaction.[51,87] One could argue that the addition of MnO to a cobalt-based FTS catalyst makes the catalyst more similar to iron-based systems.

MSIs provide an opportunity to enhance the FTS activity and even to tweak the selectivity, when carefully orchestrated. They could create interfaces with special properties or simply alter the reducibility of the metal nanoparticles.

THE COBALT/TiO_2 SHOWCASE

In this section, the active and deactivating phases in the cobalt/TiO_2 FTS catalyst will be comprehensively discussed. Cobalt supported on TiO_2 is of great importance in FTS, both in academic and industrial settings. TiO_2 was first mentioned by Tauster et al.[151,152] in the 1980s as an activity-enhancing support in the FTS reaction. Since then, many scientists have been elucidating the underlying reasons for this behavior. Our research group has contributed to the better understanding of the cobalt/TiO_2 system in FTS,[13,81,83,84,86,87,119,120,163,164] using advanced spectroscopic characterization techniques, such as XRD,[13,165] X-ray absorption spectroscopy (XAS),[81,86,164,165] Raman spectroscopy,[13] scanning transmission X-ray microscopy (STXM),[10,120] and X-ray Raman scattering (XRS) spectroscopy,[11] under realistic reaction conditions.

The cobalt/TiO_2 catalyst is an intricate system. As briefly discussed before, TiO_2 is a reducible metal oxide that actively participates in the formation of the active phase under FTS reaction conditions. The three most common crystal phases of TiO_2 are anatase (tetragonal), brookite (orthorhombic), and rutile (tetragonal).[166] The phases can be distinguished, for example, with vibrational spectroscopy[166] or XRD.[167] Often mixtures of the two tetragonal crystal phases, such as P90 (90% anatase, 10% rutile),[10,11] are used in heterogeneous catalysis. Both anatase and rutile TiO_2 can already be reduced to TiO_{2-x} suboxide species in H_2 at temperatures above 300°C.[100] These suboxides interact electronically with the cobalt nanoparticles, leading to the formation of interfaces with special properties, e.g., enhanced FTS activity.[151,152] However, if these MSIs are too strong, TiO_{2-x} suboxide species may block active sites or $CoTiO_3$ may be formed.[21] This inactive metal-support compound is more likely to be formed at high CO conversions and when cobalt oxides are present in the catalyst under reaction conditions. The latter is because positively charged Co^{2+} more readily accepts an electron than Co^0. With the cobalt/TiO_2 system, it is thus only a fine line between enhanced activity and deactivation.

The first step toward understanding these special interfaces is detecting and characterizing them in detail, preferably under relevant reaction conditions. X-ray-based techniques are promising, because they are element specific and sensitive to the direct surroundings of atoms (i.e., local bonds and oxidation state). Nevertheless, experiments with cobalt/TiO_2 can be challenging due to the relatively short attenuation length, which is element specific as well, of TiO_2 (Figure 8A). The intensity of the X-ray beam is diminished as it traverses through the material, mainly caused by strong absorption of photons by TiO_2. The attenuation length before the Ti L-edge is ~600 nm, while at the carbon K-edge, oxygen K-edge, and cobalt L-edge it is only ~200–350 nm. At the Ti K-edge and cobalt K-edge it can reach up to ~9 and 18 μm, respectively. Typically, X-ray-based techniques such as STXM or transmission X-ray microscopy (TXM) (Figures 8B and 9C) and XAS (Figures 8C and 9E) are

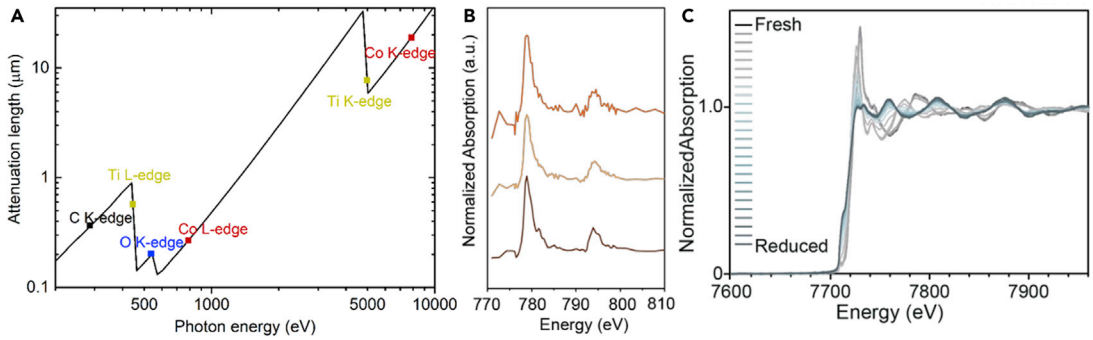

Figure 8. X-ray spectroscopy characterization of cobalt/TiO2

(A) X-ray attenuation length at the carbon K-, Ti L-, oxygen K-, cobalt L-, Ti K-, and cobalt K-edge. The TiO_2 density was set at 3.9 g/cm^3 and the beam incident angle at 90°. Calculated via CXRO.[170]

(B) Cobalt L2,3-edge spectra of a 15 wt % cobalt/TiO_2 catalyst particle after reduction in H_2 as measured with *in situ* STXM. Reprinted with permission from van Ravenhorst et al.[10] Copyright (2018) John Wiley and Sons.

(C) Cobalt K-edge spectra of a 15 wt % cobalt/TiO_2 catalyst during reduction in H_2 as measured with *in situ* XAS. Reprinted with permission from Cromer et al.[167] Copyright (2021) American Chemical Society.

measured in transmission mode. Particularly when measuring in the soft X-ray regime (50–2000 eV[168]), the sample thickness is thus limited to 200–600 nm in order to obtain a decent signal-to-noise ratio. Besides, bulk characterization techniques do not suffice for detecting and characterizing low-concentration interfaces. A surface-sensitive or nanoscale chemical imaging technique, such as high-resolution STXM[10,119,168] or TXM,[119,120,169] needs to be employed (Figures 9C and 9D).

Furthermore, the widely used vibrational spectroscopy techniques IR and Raman (micro)spectroscopy are promising tools. These techniques are based on the principle that molecules absorb or scatter specific frequencies of light that correspond to the vibrational frequencies of their unique bonds. However, those techniques can be complicated due to the strong absorption of IR and visible light by the black cobalt/TiO_2 system. Besides, the reduced TiO_2 suboxide species (TiO_{2-x}) exhibit high IR and visible light absorption activity. This is beneficial for photocatalytic applications[171] but becomes problematic during vibrational spectroscopy experiments under FTS reaction conditions. Moreover, the need for a surface-sensitive or nanoscale chemical imaging technique applies to vibrational spectroscopy as well. The spatial resolutions of both IR and Raman spectroscopy are limited by the wavelength. For Raman spectroscopy, this is in the range of several hundreds of nanometers (e.g., 532 nm[13]), but for IR spectroscopy the wavelength ranges from 1 μm to 1,000 μm. The diffraction limitations can be overcome by combining vibrational spectroscopy with scanning probe techniques, such as atomic force microscopy (AFM).[172,173] Examples of this include AFM-Raman, tip-enhanced Raman spectroscopy (TERS),[174,175] AFM-IR, and photo-induced force microscopy (PiFM).[172,176] Using such state-of-the-art methods under FTS reaction conditions is extremely challenging and, although developments are ongoing,[173,177] we still have a long road ahead.

Apart from the special interfaces between cobalt and TiO_2, carbide formation and carbon deposition are important to detect and characterize. Both cobalt carbide formation and carbon deposition are phenomena that start at the catalyst surface under FTS reaction conditions. Bulk characterization techniques may again be insufficient to detect these phenomena at an early stage. Soft X-ray spectroscopy techniques can detect carbon species by measuring at the carbon K-edge (~280 eV) and may offer a solution. Surface-sensitive techniques, such as XPS (Figure 9B),[22,103,178]

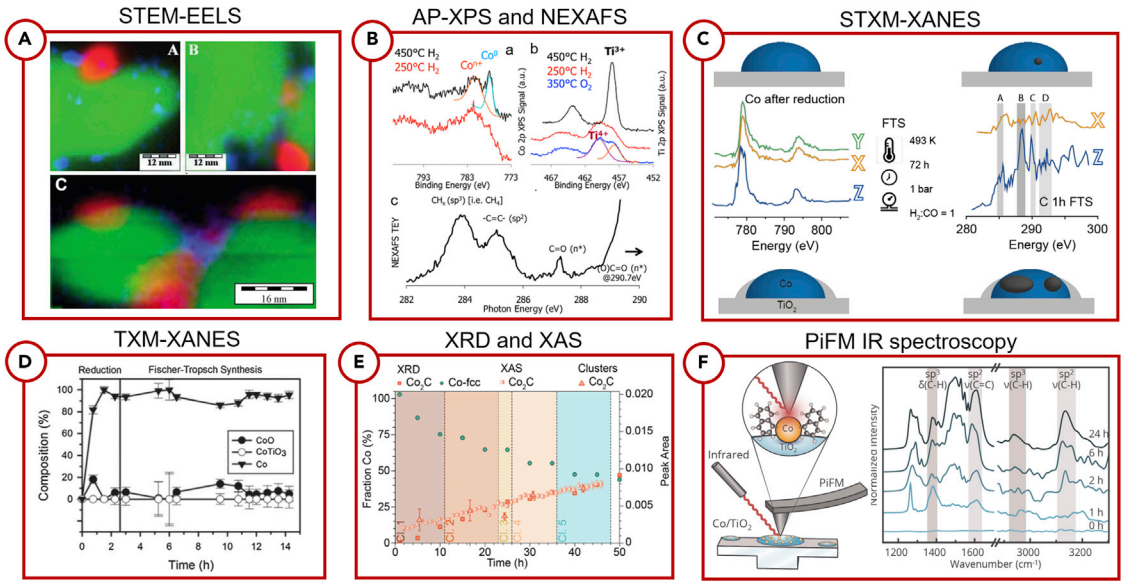

Figure 9. Overview of promising techniques used and results obtained for cobalt/TiO_2 from different studies

(A) Scanning transmission electron microscopy (STEM) electron energy loss spectroscopy (EELS) results on a reduced CoMn/TiO_2 catalyst, showing interfaces between cobalt and titania. Reproduced from Morales et al.[83,84] with permission from the PCCP Owner Societies.

(B) Ambient pressure (AP) XPS at (a) cobalt 2p and (b) Ti 2p core levels under the given conditions, as well as (c) *in situ* near-edge X-ray absorption fine-edge structure (NEXAFS) results at the carbon K edge under CO_2 hydrogenation conditions (T = 250°C, P = 1 bar, H_2/CO_2 = 3). Reprinted with permission from Melaet et al.[22] Copyright (2014) American Chemical Society.

(C) Operando STXM X-ray absorption near-edge structure (XANES) results on a cobalt/TiO_2 catalyst under FTS reaction conditions (T = 220°C, P = 1 bar, H_2/CO = 1). The cobalt L edge (left) shows that particles X and Y contain metallic cobalt, whereas particle Z is slightly oxidized. As a result, particle Z forms more carbon deposits (carbon K-edge, right) compared with particles X and Y. Reprinted with permission from van Ravenhorst et al.[10] Copyright (2018) John Wiley and Sons.

(D) *In situ* TXMXANES results indicating the cobalt phases present in a cobalt/TiO_2 catalyst particle under FTS reaction conditions (T = 250°C, P = 10 bar, H_2/CO = 2). Reproduced from Cats et al.[120] with permission from The Royal Society of Chemistry.

(E) Operando XRD and XAS results on a cobalt/TiO_2 catalyst indicating the cobalt phases present under FTS reaction conditions (T = 220°C, P = 16 bar, H_2/CO = 1). Reprinted with permission from Cromer et al.[167] Copyright (2021) American Chemical Society.

(F) Scanning probe vibrational spectroscopy: PiFM IR spectroscopy to detect carbon species on a cobalt/TiO_2 FTS catalyst post FTS (T = 220°C, P = 1 bar, H_2/CO = 2).

and nanoscale chemical imaging techniques, such as STXM (Figure 9C),[10] proved to suffice even under FTS reaction conditions. Carbon deposition was linked to an increased selectivity toward the desired long-chain hydrocarbon products.[103] Scanning probe vibrational spectroscopy techniques (Figure 9F) are promising for detecting surface carbides and carbon deposition as well. However, employing these techniques under realistic FTS conditions is challenging and still in its infancy.

Resolving the debate regarding the active and deactivating phases in cobalt-based FTS has been, and still remains, challenging. The main issues we need to address more clearly in the open literature are the catalyst synthesis procedure and the resulting catalyst properties, such as cobalt nanoparticle size, the properties of the support material, and the reaction conditions. Besides, clarifying speculations regarding surface and/or interface phenomena, such as special interfaces between cobalt and TiO_2, requires surface-sensitive and/or nanoscale chemical imaging techniques under relevant FTS reaction conditions. Progress with X-ray-based techniques has certainly been made over the past few decades,[10,120,122] but developments are still ongoing in the field of scanning probe vibrational spectroscopy.[173] An overview highlighting promising characterization techniques and results obtained on cobalt/TiO_2 can be found in Figure 9.

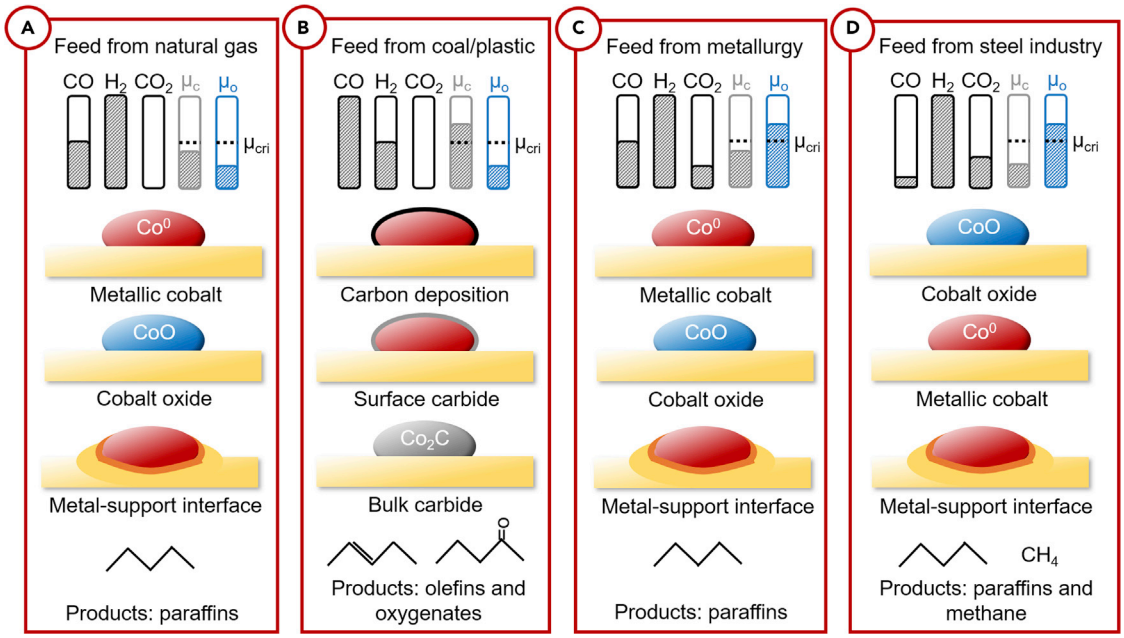

Figure 10. Overview of the chemical potentials μ_c and μ_o under FTS conditions

The syngas composition, which is dependent on the feedstock, determines the cobalt active phase under reaction conditions and the final products that are formed. Syngas prepared from (A) natural gas ($H_2/CO = 2$); metallic cobalt is present under these conditions and potentially some cobalt oxide and/or metal-support interfaces.

(B) Coal, plastic, or municipal waste ($H_2/CO \leq 1$); carbon deposition is likely formed under these conditions, as well as surface and/or bulk cobalt carbide.

(C) Metallurgy ($H_2/CO/CO_2$ with $[CO]>[CO_2]$); metallic cobalt, cobalt oxide, and potentially metal-support interfaces are present under these conditions.

(D) Steel production ($H_2/CO/CO_2$ with $[CO]<[CO_2]$); metallic cobalt, cobalt oxide, and potentially metal-support interfaces are present under these conditions.

Nevertheless, based on the discussion above, we can now briefly summarize some general findings regarding the active and deactivating phases in the cobalt/TiO_2 FTS system. The catalytically active phases in the cobalt/TiO_2 FTS catalyst are metallic cobalt,[2,21] the interface between metallic cobalt or cobalt oxide and TiO_2,[22] and metallic cobalt with atomic or amorphous carbon deposition.[10,31] The deactivating phases are $CoTiO_3$[21] and metallic cobalt with graphitic carbon deposition, which specifically inhibits methane formation.[103] Cobalt carbides can be active in FTS and selective toward olefins and oxygenates, provided that they are stabilized by an oxidic compound[52,91,92,94,96,139,143] and/or alkali promoter.[53,91] The active cobalt phase under FTS reaction conditions is dependent on the composition of the syngas feed, which determines both the chemical potentials of carbon (μ_c) and oxygen (μ_o). When the chemical potentials are higher than the critical chemical potential (μ_{cri}), a phase transition can take place.[97,179] For example, when $\mu_c>\mu_{cri}$ cobalt carbide will be formed and when $\mu_o>\mu_{cri}$ cobalt oxide will be formed. In the classical cobalt-based FTS scenario, the syngas feed is produced from natural gas and has $H_2/CO = 2$ (Figure 10A). Metallic cobalt is the main active phases under such conditions, while some cobalt oxide and metal-support interfaces could be present as well. Linear paraffin products are then the output of the reaction. Under high CO conversion conditions, large amounts of water may deactivate the catalyst via, e.g., sintering, oxidation, or the formation of inactive metal-support compounds.[21] If coal, plastic, and potentially municipal waste are used as feedstock, the syngas contains typically more CO; e.g.; $H_2/CO \leq 1$ (Figure 10B). Under such reaction conditions, carbon deposition is often formed and possibly surface and/or bulk cobalt carbide, as

Table 1. Proposed active and inactive phases in the cobalt-based FTS

Phase	Short description	Active	Inactive
Metallic cobalt	metallic cobalt is formed in the catalyst during reduction in H_2 and is the most widely accepted active phase in FTS	2,18,21,35,37,43,100,162,181,182	N/A
Cobalt oxides	cobalt oxides often coexist with metallic cobalt in the catalyst under FTS reaction conditions. The presence of water promotes re-oxidation of small cobalt nanoparticles	22,51,101,102	1,21,123,124
Cobalt carbides	cobalt carbides can form under FTS reaction conditions, especially in CO-rich conditions and under high pressure. Typically an alkali or oxidic compound is needed for stabilization	52,53,91,94–97,136–138,140–142,147,165,183	1,11,13,98–100
Cobalt with carbon deposition	carbon deposition is present on the catalyst under reaction conditions. This can be in atomic, amorphous aliphatic, amorphous (poly)aromatic, or graphitic form	10,31,103	1,12,28
Metal-support interfaces	metal-support interfaces can form readily on reducible supports during reduction or FTS	22,51,86,87,94,96,151,157–160	157
Metal-support compounds	mixed-metal-support compounds can form at high CO conversion conditions in the presence of water	N/A	1,21,121–123,126

$\mu_c > \mu_{cri}$. The output then shifts to olefin and oxygenated products. Under these conditions, the CO_2 content at the reactor exit may be significant enough to induce surface oxidation. Besides, water could again lead to deactivation at high conversion rates. Waste streams from metallurgy are generally a mixture of $H_2/CO/CO_2$, with $[CO]>[CO_2]$, and could also be used as syngas (Figure 10C). Metallic cobalt is again the main active phase under such conditions, while some cobalt oxide and metal-support interfaces could also be present and paraffin products are the output. Another waste stream that could be employed as syngas comes from the steel industry. This is also a mixture of $H_2/CO/CO_2$, with $[CO]<[CO_2]$ (Figure 10D).[180] This feed, as well as the feed from metallurgy, is slightly more oxidizing due to the presence of CO_2. The active phases under these conditions are metallic cobalt or cobalt oxide and potentially metal-support interfaces. The output are paraffin products and the amount of methane likely scales with the concentration of CO_2 versus CO. For both the feeds from metallurgy and the steel industry, it is expected that water may deactivate the catalyst at high conversion rates.

SUMMARY AND OUTLOOK

The present review of the active and inactive phases in a cobalt-based FTS catalyst underlines the complexity of this catalytic system. The opinions reported in the literature are divergent. Most often, multiple phases coexist under FTS reaction conditions, which makes it challenging to correlate one specific phase to, e.g., enhanced performance or deactivation. Most researchers believe that metallic cobalt is the true active phase in FTS. However, cobalt oxides, cobalt carbides, cobalt with carbon deposition, and cobalt-support interfaces have all been reported as active phases as well. This is summarized in Table 1. However, specific terms have to be met in order for the aforementioned cobalt phases to be active in FTS:

- Cobalt oxides have only been reported as active in FTS when supported on a reducible metal oxide support.
- Cobalt carbides have been reported active in FTS and selective to olefins and/or oxygenates, provided that they are stabilized by and in synergy with an oxidic compound and/or an alkali promoter.

- Cobalt with carbon deposition has only been considered an active phase if the carbon species are atomic or amorphous and can be removed from the surface by hydrogenation below 350°C.
- Cobalt-support interfaces have been reported to enhance the FTS activity, when the support was a reducible metal oxide and given that the interactions were not too strong. Oxidic promoter elements have also been reported to form interfaces with cobalt that display enhanced FTS activity.

If these terms are not met, the cobalt phases mentioned above are often reported as inactive or deactivating in FTS. Additionally, cobalt with irreversible carbon deposition and cobalt-support compounds have exclusively been reported as deactivating in FTS. Catalyst deactivation is a multifaceted process and under reaction conditions and it is likely that different mechanisms play a role in the overall deteriorating catalyst activity and selectivity. Over the past decade, progress has been made with surface-sensitive and nanoscale chemical imaging techniques under reaction conditions (*in situ*), while monitoring the activity and selectivity (*operando*). Besides, long-term deactivation studies, both with synchrotron and laboratory-based techniques, have been enabled by close collaborations between industry and academia. Examples of such collaborations are investigating actual commercial catalysts and designing reactors for spectroscopic studies under industrially relevant reaction conditions. All of this has contributed tremendously to our understanding of the active and inactive phases in cobalt-based FTS. However, promising developments likely leading to new insights, for example with scanning probe vibrational spectroscopy, are still ongoing.

ACKNOWLEDGMENTS

The Netherlands Research Council (NWO) is acknowledged for financial support in the frame of a Technology Area (TA) grant of the Innovation Fund Chemistry, together with Shell Global Solutions International B.V., DSM Resolve, and Leiden Probe Microscopy. Prof. Dr. E.T.C. Vogt is gratefully acknowledged for providing the crystal structures and XRD patterns in Figure 6.

AUTHOR CONTRIBUTIONS

B.M.W. proposed the topic of the review and supervised the writing process. I.C.t.H. wrote and revised the manuscript.

DECLARATION OF INTERESTS

The authors declare no competing interests.

REFERENCES

1. Tsakoumis, N.E., Rønning, M., Borg, Ø., Rytter, E., and Holmen, A. (2010). Deactivation of cobalt based Fischer-Tropsch catalysts: a review. Catal. Today *154*, 162–182.

2. van de Loosdrecht, J., Botes, F.G., Ciobica, I.M., Ferreira, A., Gibson, P., Moodley, D.J., Saib, A.M., Visagie, J.L., Weststrate, C.J., and Niemantsverdriet, J.W. (2013). Fischer-Tropsch synthesis: catalysts and chemistry. Compreh. Inorg. Chem. II *7*, 525–557.

3. Luk, H.T., Mondelli, C., Ferre, C., Stewart, J.A., and Pe, J. (2016). Status and prospects in higher alcohols synthesis from syngas. Chem. Soc. Rev. *46*, 1358–1426.

4. Fischer, F., and Tropsch, H. (1923). The preparation of synthetic oil mixtures (synthol) from carbon monoxide and hydrogen. Brennst.-Chem. *4*, 276–285.

5. Fischer, F., and Tropsch, H. (1926). The synthesis of petroleum at atmospheric pressures from gasification products of coal. Brennst.-Chem. *7*, 97–104.

6. Ye, R.P., Ding, J., Gong, W., Argyle, M.D., Zhong, Q., Wang, Y., Russell, C.K., Xu, Z., Russell, A.G., Li, Q., et al. (2019). CO_2 hydrogenation to high-value products via heterogeneous catalysis. Nat. Commun. *10*, 5698.

7. Li, J., He, Y., Tan, L., Zhang, P., Peng, X., Oruganti, A., Yang, G., Abe, H., Wang, Y., and Tsubaki, N. (2018). Integrated tuneable synthesis of liquid fuels via Fischer–Tropsch technology. Nat. Catal. *1*, 787–793.

8. Li, W., Wang, H., Jiang, X., Zhu, J., Liu, Z., Guo, X., and Song, C. (2018). A short review of recent advances in CO_2 hydrogenation to hydrocarbons over heterogeneous catalysts. RSC Adv. *8*, 7651–7669.

9. De Smit, E., and Weckhuysen, B.M. (2008). The renaissance of iron-based Fischer-Tropsch synthesis: on the multifaceted catalyst deactivation behaviour. Chem. Soc. Rev. *37*, 2758–2781.

10. van Ravenhorst, I.K., Vogt, C., Oosterbeek, H., Bossers, K.W., Moya-Cancino, J.G., van Bavel, A.P., van der Eerden, A.M.J., Vine, D., de Groot, F.M.F., Meirer, F., et al. (2018). Capturing the genesis of an active Fischer–Tropsch synthesis catalyst with operando X-ray nanospectroscopy. Angew. Chem. Int. Ed. *57*, 11957–11962.

11. Moya-Cancino, J.G., Honkanen, A., van der Eerden, A.M.J., Oord, R., Monai, M., ten Have, I.C., Sahle, C.J., Meirer, F., Weckhuysen, B.M., and de Groot, F.M.F. (2021). In situ X-ray Raman scattering spectroscopy of the formation of cobalt carbides in a Co/TiO_2 Fischer−Tropsch synthesis catalyst. ACS Catal. *11*, 809–819.

12. Moodley, D.J., van de Loosdrecht, J., Saib, A.M., Overett, M.J., Datye, A.K., and Niemantsverdriet, J.W. (2009). Carbon deposition as a deactivation mechanism of cobalt-based Fischer-Tropsch synthesis catalysts under realistic conditions. Appl. Catal. A Gen. *354*, 102–110.

13. Cats, K.H., and Weckhuysen, B.M. (2016). Combined operando X-ray diffraction/Raman spectroscopy of catalytic solids in the laboratory: the Co/TiO_2 Fischer-Tropsch synthesis catalyst showcase. ChemCatChem *8*, 1531–1542.

14. Loewert, M., Serrer, M.A., Carambia, T., Stehle, M., Zimina, A., Kalz, K.F., Lichtenberg, H., Saraçi, E., Pfeifer, P., and Grunwaldt, J.D. (2020). Bridging the gap between industry and synchrotron: an operando study at 30 bar over 300 h during Fischer-Tropsch synthesis. React. Chem. Eng. *5*, 1071–1082.

15. Böller, B., Durner, K.M., and Wintterlin, J. (2019). The active sites of a working Fischer–Tropsch catalyst revealed by operando scanning tunnelling microscopy. Nat. Catal. *2*, 1027–1034.

16. van Santen, R.A., Ciobîcâ, I.M., van Steen, E., and Ghouri, M.M. (2011). Mechanistic issues in Fischer-Tropsch catalysis. Adv. Catal. *54*, 127–187.

17. Zijlstra, B., Broos, R.J.P., Chen, W., Bezemer, G.L., Filot, I.A.W., and Hensen, E.J.M. (2020). The vital role of step-edge sites for both CO activation and chain growth on cobalt Fischer-Tropsch catalysts revealed through first-principles-based microkinetic modeling including lateral interactions. ACS Catal. *10*, 9376–9400.

18. Weststrate, C.J., Sharma, D., Garcia Rodriguez, D., Gleeson, M.A., Fredriksson, H.O.A., and Niemantsverdriet, J.W.H. (2020). Mechanistic insight into carbon-carbon bond formation on cobalt under simulated Fischer-Tropsch synthesis conditions. Nat. Commun. *11*, 750.

19. Inderwildi, O.R., Jenkins, S.J., and King, D.A. (2008). Fischer-Tropsch mechanism revisited: alternative pathways for the production of higher hydrocarbons from synthesis gas. J. Phys. Chem. C *112*, 1305–1307.

20. Weststrate, C.J., Gericke, H.J., Verhoeven, M.W.G.M., Ciobîcă, I.M., Saib, A.M., and Niemantsverdriet, J.W. (2010). Ethanol decomposition on Co(0001): C-O bond scission on a close-packed cobalt surface. J. Phys. Chem. Lett. *1*, 1767–1770.

21. Wolf, M., Fischer, N., and Claeys, M. (2020). Water-induced deactivation of cobalt-based Fischer–Tropsch catalysts. Nat. Catal. *3*, 962–965.

22. Melaet, G., Ralston, W.T., Li, C.S., Alayoglu, S., An, K., Musselwhite, N., Kalkan, B., and Somorjai, G.A. (2014). Evidence of highly active cobalt oxide catalyst for the Fischer-Tropsch synthesis and CO_2 hydrogenation. J. Am. Chem. Soc. *136*, 2260–2263.

23. Paalanen, P.P., van Vreeswijk, S.H., and Weckhuysen, B.M. (2020). Combined in situ X-ray powder diffractometry/Raman spectroscopy of iron carbide and carbon species evolution in Fe(-Na-S)/α-Al_2O_3 catalysts during Fischer-Tropsch synthesis. ACS Catal. *10*, 9837–9855.

24. Paalanen, P.P., van Vreeswijk, S.H., Dugulan, A.I., and Weckhuysen, B.M. (2020). Identification of iron carbides in Fe(−Na−S)/α-Al_2O_3 Fischer-Tropsch synthesis catalysts with X-ray powder diffractometry and Mössbauer absorption spectroscopy. ChemCatChem *12*, 5121–5139.

25. Rahmati, M., Safdari, M.S., Fletcher, T.H., Argyle, M.D., and Bartholomew, C.H. (2020). Chemical and thermal sintering of supported metals with emphasis on cobalt catalysts during Fischer-Tropsch synthesis. Chem. Rev. *120*, 4455–4533.

26. Bartholomew, C.H. (2001). Mechanisms of catalyst deactivation. Appl. Catal. A Gen. *212*, 17–60.

27. van Deelen, T.W., Hernández Mejía, C., and de Jong, K.P. (2019). Control of metal-support interactions in heterogeneous catalysts to enhance activity and selectivity. Nat. Catal. *2*, 955–970.

28. Weststrate, C.J., Ciobîcă, I.M., Saib, A.M., Moodley, D.J., and Niemantsverdriet, J.W. (2014). Fundamental issues on practical Fischer-Tropsch catalysts: how surface science can help. Catal. Today *228*, 106–112.

29. Wang, Z., Yan, Z., Liu, C., and Goodman, D.W. (2011). Surface science studies on cobalt Fischer-Tropsch catalysts. ChemCatChem *3*, 551–559.

30. Oosterbeek, H. (2007). Bridging the pressure and material gap in heterogeneous catalysis: cobalt Fischer–Tropsch catalysts from surface science to industrial application. Phys. Chem. Chem. Phys. *9*, 3570–3576.

31. Weststrate, C.J., Kazalkaya, A.C., Rossen, E.T.R., Verhoeven, M.W.G.M., Ciobîcă, I.M., Saib, A.M., and Niemantsverdriet, J.W. (2012). Atomic and polymeric carbon on Co(0001): surface reconstruction, graphene formation, and catalyst poisoning. J. Phys. Chem. C *116*, 11575–11583.

32. Bell, A.T., Bond, G.C., Thompson, D.T., Valden, M., Lai, X., Goodman, D.W., Blasko, T., Nieto, J.M.L., Chen, K., Bell, A.T., et al. (2003). The impact of nanoscience on heterogeneous catalysis. Science *299*, 1688–1691.

33. Navarro, V., van Spronsen, M.A., and Frenken, J.W.M. (2016). In situ observation of self-assembled hydrocarbon Fischer-Tropsch products on a cobalt catalyst. Nat. Chem. *8*, 929–934.

34. Weststrate, C.J., van Helden, P., and Niemantsverdriet, J.W. (2016). Reflections on the Fischer-Tropsch synthesis: mechanistic issues from a surface science perspective. Catal. Today *275*, 100–110.

35. Price, S.W.T., Martin, D.J., Parsons, A.D., Sławiński, W.A., Vamvakeros, A., Keylock, S.J., Beale, A.M., and Mosselmans, J.F.W. (2017). Chemical imaging of Fischer-Tropsch catalysts under operating conditions. Sci. Adv. *3*, e1602838.

36. Hoffman, A.S., Singh, J.A., Bent, S.F., and Bare, S.R. (2018). In situ observation of phase changes of a silica-supported cobalt catalyst for the Fischer-Tropsch process by the development of a synchrotron-compatible in situ/operando powder X-ray diffraction cell. J. Synchrotron Radiat. *25*, 1673–1682.

37. Qi, Z., Chen, L., Zhang, S., Su, J., and Somorjai, G.A. (2020). A mini review of cobalt-based nanocatalyst in Fischer-Tropsch synthesis. Appl. Catal. A Gen. *602*, 117701.

38. Storch, H.H., Anderson, R.A., and Golumbic, N. (1951). The Fischer-Tropsch and Related Syntheses: Including a Summary of Theoretical and Applied Contact Catalysis (Wiley).

39. Anderson, R.B. (1956). Catalysts for the Fischer-Tropsch synthesis. Catalysis *4*, 29–255.

40. Chen, W., Filot, I.A.W., Pestman, R., and Hensen, E.J.M. (2017). Mechanism of cobalt-catalyzed CO hydrogenation: 2. Fischer–Tropsch synthesis. ACS Catal. *7*, 8061–8071.

41. Hindermann, J.P., Hutchings, G.J., and Kiennemann, A. (1993). Mechanistic aspects of the formation of hydrocarbons and alcohols from CO hydrogenation. Catal. Rev. Eng. *35*, 1–127.

42. Chen, W., Pestman, R., Zijlstra, B., Filot, I.A.W., and Hensen, E.J.M. (2017). Mechanism of cobalt-catalyzed CO hydrogenation: 1. Methanation. ACS Catal. *7*, 8050–8060.

43. Lyu, S., Wang, L., Zhang, J., Liu, C., Sun, J., Peng, B., Wang, Y., Rappé, K.G., Zhang, Y., Li, J., et al. (2018). Role of active phase in Fischer-Tropsch synthesis: experimental evidence of CO activation over single-phase cobalt catalysts. ACS Catal. *8*, 7787–7798.

44. Pestman, R., Chen, W., and Hensen, E. (2019). Insight into the rate-determining step and active sites in the Fischer-Tropsch reaction over cobalt catalysts. ACS Catal. *9*, 4189–4195.

45. Filot, I.A.W., van Santen, R.A., and Hensen, E.J.M. (2014). The optimally performing Fischer-Tropsch catalyst. Angew. Chem. Int. Ed. *53*, 12746–12750.

46. Zijlstra, B., Broos, R.J.P., Chen, W., Oosterbeek, H., Filot, I.A.W., and Hensen, E.J.M. (2019). Coverage effects in CO dissociation on metallic cobalt nanoparticles. ACS Catal. *9*, 7365–7372.

47. Zijlstra, B., Broos, R.J.P., Chen, W., Filot, I.A.W., and Hensen, E.J.M. (2020). First-principles based microkinetic modeling of transient kinetics of CO hydrogenation on cobalt catalysts. Catal. Today *342*, 131–141.

48. Lindsay, D., and Kerr, W. (2011). Cobalt close-up. Nat. Chem. *3*, 494.

49. Greenwood, N.N., and Earnshaw, A. (2012). Cobalt, rhodium and iridium. In Chemistry of the Elements (Elsevier), pp. 1113–1143.

50. Lu, X., Heal, K.R., Ingalls, A.E., Doxey, A.C., and Neufeld, J.D. (2020). Metagenomic and chemical characterization of soil cobalamin production. ISME J. *14*, 53–66.

51. Li, C.S., Melaet, G., Ralston, W.T., An, K., Brooks, C., Ye, Y., Liu, Y.S., Zhu, J., Guo, J., Alayoglu, S., et al. (2015). High-performance hybrid oxide catalyst of manganese and cobalt for low-pressure methanol synthesis. Nat. Commun. *6*, 6538.

52. Lin, T., Gong, K., Wang, C., An, Y., Wang, X., Qi, X., Li, S., Lu, Y., Zhong, L., and Sun, Y. (2019). Fischer-Tropsch synthesis to olefins: catalytic performance and structure evolution of Co_2C-based catalysts under a CO_2 environment. ACS Catal. *9*, 9554–9567.

53. Zhang, S., Liu, X., Shao, Z., Wang, H., and Sun, Y. (2020). Direct CO_2 hydrogenation to ethanol over supported Co_2C catalysts: studies on support effects and mechanism. J. Catal. *382*, 86–96.

54. Zhang, Q., Deng, W., and Wang, Y. (2013). Recent advances in understanding the key catalyst factors for Fischer-Tropsch synthesis. J. Energy Chem. *22*, 27–38.

55. Sabatier, P., and Senderens, J.B. (1902). Direct hydrogenation of oxides of carbon in presence of various finely divided metals. CR Acad. Sci. *134*, 689–691.

56. Fischer, F., and Tropsch, H. (1925). Verfahren zur Gewinnung mehrgliedriger Paraffinkohlenwasserstoffe aus Kohlenoxyden und Wasserstoff auf katalytischem Wege, Patent DE 484337.

57. Fischer, F., and Tropsch, H. (1930). Process for the Production of Paraffin-Hydrocarbons with More than One Carbon Atom, US Patent 1746464.

58. Craxford, S.R., and Rideal, E.K. (1939). The mechanism of the synthesis of hydrocarbons from water gas. J. Chem. Soc. *338*, 1604–1614.

59. Storch, H.H. (1945). Catalysis in synthetic liquid-fuel processes. Ind. Eng. Chem. *37*, 340–351.

60. Herington, E.F.G., and Woodward, L.A. (1939). Experiments on the Fischer-Tropsch synthesis of hydrocarbons from carbon monoxide and hydrogen. Trans. Faraday Soc. *35*, 958–966.

61. Hamai, S. (1941). Physico-chemical investigations on catalytic mechanism. II. Note on the Fischer-Tropsch synthesis of hydrocarbons with special reference to its reaction mechanism. Bull. Chem. Soc. Jpn. *16*, 213–228.

62. Hofer, L.J.E., and Peebles, W.C. (1947). X-ray diffraction studies of the action of carbon monoxide on cobalt-Thoria-Kieselguhr catalysts. J. Am. Chem. Soc. *69*, 2497–2500.

63. Weller, S., Hofer, L.J.E., Anderson, R.B., Weller, S., Hofer, L.J.E., and Anderson, R.B. (1948). The role of bulk cobalt carbide in the Fischer-Tropsch synthesis. J. Am. Chem. Soc. *70*, 799–801.

64. Kummer, J.T., DeWitt, T.W., and Emmett, P.H. (1948). Some mechanism studies on the Fischer-Tropsch synthesis using C^{14}. J. Am. Chem. Soc. *70*, 3632–3643.

65. Mattox, W.J. (1950). Process of Regenerating a Fluidized Fischer-Tropsch Catalyst. US Patent, 2,515,245.

66. Blyholder, G., and Emmett, P.H. (1959). Fischer-Tropsch synthesis mechanism studies. The addition of radioactive ketene to the synthesis gas. J. Phys. Chem. *63*, 962–965.

67. Biloen, P., and Sachtler, W.M.H. (1981). Mechanism of hydrocarbon synthesis over Fischer-Tropsch catalysts. Adv. Catal. *30*, 165–216.

68. Reuel, R.C., and Bartholomew, C.H. (1984). Effects of support and dispersion on the CO hydrogenation activity/selectivity properties of cobalt. J. Catal. *85*, 78–88.

69. Reuel, R.C., and Bartholomew, C.H. (1984). The stoichiometries of H_2 and CO adsorptions on cobalt: effects of support and preparation. J. Catal. *85*, 63–77.

70. Bessell, S. (1993). Support effects in cobalt-based Fischer-Tropsch catalysis. Appl. Catal. A Gen. *96*, 253–268.

71. Kogelbauer, A., Weber, J.C., and Goodwin, J.G. (1995). The formation of cobalt silicates on Co/SiO_2 under hydrothermal conditions. Catal. Lett. *34*, 259–267.

72. van de Loosdrecht, J., van der Haar, M., van der Kraan, A.M., van Dillen, A.J., and Geus, J.W. (1997). Preparation and properties of supported cobalt catalysts for Fischer-Tropsch synthesis. Appl. Catal. A Gen. *150*, 365–376.

73. Ming, H., and Baker, B.G. (1995). Characterization of cobalt Fischer-Tropsch catalysts I. Unpromoted cobalt-silica gel catalysts. Appl. Catal. A Gen. *123*, 23–36.

74. Khodakov, A.Y., Lynch, J., Bazin, D., Rebours, B., Zanier, N., Moisson, B., and Chaumette, P. (1997). Reducibility of cobalt species in silica-supported Fischer-Tropsch catalysts. J. Catal. *168*, 16–25.

75. Ernst, B., Libs, S., Chaumette, P., and Kiennemann, A. (1999). Preparation and characterization of Fischer–Tropsch active Co/SiO_2 catalysts. Appl. Catal. A Gen. *186*, 145–168.

76. Khodakov, A.Y. (2009). Fischer-Tropsch synthesis: relations between structure of cobalt catalysts and their catalytic performance. Catal. Today *144*, 251–257.

77. Saib, A.M., Claeys, M., and van Steen, E. (2002). Silica supported cobalt Fischer-Tropsch catalysts: effect of pore diameter of support. Catal. Today *71*, 395–402.

78. Khodakov, A.Y., Bechara, R., and Griboval-Constant, A. (2003). Fischer-Tropsch synthesis over silica supported cobalt catalysts: mesoporous structure versus cobalt surface density. Appl. Catal. A Gen. *254*, 273–288.

79. Soled, S.L., Iglesia, E., Fiato, R.A., Baumgartner, J.E., Vroman, H., and Miseo, S. (2003). Control of metal dispersion and structure by changes in the solid-state chemistry of supported cobalt Fischer-Tropsch catalysts. Top. Catal. *26*, 101–109.

80. Enache, D.I., Roy-Auberger, M., and Revel, R. (2004). Differences in the characteristics and catalytic properties of cobalt-based Fischer-Tropsch catalysts supported on zirconia and alumina. Appl. Catal. A Gen. *268*, 51–60.

81. Morales, F., de Groot, F.M.F., Glatzel, P., Kleimenov, E., Bluhm, H., Hävecker, M., Knop-Gericke, A., and Weckhuysen, B.M. (2004). In situ X-ray absorption of $Co/Mn/TiO_2$ catalysts for Fischer–Tropsch synthesis. J. Phys. Chem. B *108*, 16201–16207.

82. Morales Cano, F., Gijzeman, O.L.J., De Groot, F.M.F., and Weckhuysen, B.M. (2004). Manganese promotion in cobalt-based Fischer-Tropsch catalysis. Stud. Surf. Sci. Catal. *147*, 271–276.

83. Morales, F., De Groot, F.M.F., Gijzeman, O.L.J., Mens, A., Stephan, O., and Weckhuysen, B.M. (2005). Mn promotion effects in Co/TiO_2 Fischer-Tropsch catalysts as investigated by XPS and STEM-EELS. J. Catal. *230*, 301–308.

84. Morales, F., Grandjean, D., de Groot, F.M., Stephan, O., and Weckhuysen, B.M. (2005). Combined EXAFS and STEM-EELS study of the electronic state and location of Mn as promoter in Co-based Fischer–Tropsch catalysts. Phys. Chem. Chem. Phys. *7*, 568–572.

85. Morales, F., and Weckhuysen, B.M. (2006). Promotion effects in Co-based Fischer–Tropsch catalysis. Catalysis *19*, 1–40.

86. Morales, F., Grandjean, D., Mens, A., De Groot, F.M.F., and Weckhuysen, B.M. (2006). X-ray absorption spectroscopy of $Mn/Co/TiO_2$ Fischer-Tropsch catalysts: relationships between preparation method, molecular structure, and catalyst performance. J. Phys. Chem. B *110*, 8626–8639.

87. Morales, F., de Smit, E., de Groot, F.M.F., Visser, T., and Weckhuysen, B.M. (2007). Effects of manganese oxide promoter on the CO and H_2 adsorption properties of titania-supported cobalt Fischer-Tropsch catalysts. J. Catal. *246*, 91–99.

88. Saib, A.M., Moodley, D.J., Ciobîc, I.M., Hauman, M.M., Sigwebela, B.H., Weststrate, C.J., Niemantsverdriet, J.W., and van de Loosdrecht, J. (2010). Fundamental understanding of deactivation and regeneration of cobalt Fischer-Tropsch synthesis catalysts. Catal. Today *154*, 271–282.

89. van Hardeveld, R., and Hartog, F. (1969). The statistics of surface atoms and surface sites on metal crystals. Surf. Sci. *15*, 189–230.

90. van Hardeveld, R., and van Montfoort, A. (1966). The influence of crystallite size on the adsorption of molecular nitrogen on nickel, palladium and platinum: an infrared and electron-microscopic study. Surf. Sci. *4*, 396–430.

91. Xiang, Y., and Kruse, N. (2016). Tuning the catalytic CO hydrogenation to straight-and long-chain aldehydes/alcohols and olefins/paraffins. Nat. Commun. *7*, 13058.

92. Zhong, L., Yu, F., An, Y., Zhao, Y., Sun, Y., Li, Z., Lin, T., Lin, Y., Qi, X., Dai, Y., et al. (2016). Cobalt carbide nanoprisms for direct production of lower olefins from syngas. Nature *538*, 84–87.

93. Yang, R., Xia, Z., Zhao, Z., Sun, F., Du, X., Yu, H., Gu, S., Zhong, L., Zhao, J., Ding, Y., et al. (2019). Characterization of CoMn catalyst by in situ X-ray absorption spectroscopy and wavelet analysis for Fischer–Tropsch to olefins reaction. J. Energy Chem. *32*, 118–123.

94. Lebarbier, V.M., Mei, D., Kim, D.H., Andersen, A., Male, J.L., Holladay, J.E., Rousseau, R., and Wang, Y. (2011). Effects of La_2O_3 on the mixed higher alcohols synthesis from syngas over Co catalysts: a combined theoretical and experimental study. J. Phys. Chem. C *115*, 17440–17451.

95. Pei, Y.P., Liu, J.X., Zhao, Y.H., Ding, Y.J., Liu, T., Dong, W. Da, Zhu, H.J., Su, H.Y., Yan, L., Li, J.L., et al. (2015). High alcohols synthesis via Fischer-Tropsch reaction at cobalt metal/carbide interface. ACS Catal. *5*, 3620–3624.

96. Gnanamani, M.K., Jacobs, G., Graham, U.M., Ribeiro, M.C., Noronha, F.B., Shafer, W.D., and Davis, B.H. (2016). Influence of carbide formation on oxygenates selectivity during Fischer-Tropsch synthesis over Ce-containing Co catalysts. Catal. Today *261*, 40–47.

97. Chen, P.P., Liu, J.X., and Li, W.X. (2019). Carbon monoxide activation on cobalt carbide for Fischer-Tropsch synthesis from first-principles theory. ACS Catal. *9*, 8093–8103.

98. Zhao, Y.H., Su, H.Y., Sun, K., Liu, J., and Li, W.X. (2012). Structural and electronic properties of cobalt carbide Co_2C and its surface stability: density functional theory study. Surf. Sci. *606*, 598–604.

99. Claeys, M., Dry, M.E., van Steen, E., du Plessis, E., van Berge, P.J., Saib, A.M., and Moodley, D.J. (2014). In situ magnetometer study on the formation and stability of cobalt carbide in Fischer-Tropsch synthesis. J. Catal. *318*, 193–202.

100. Khodakov, A.Y., Chu, W., and Fongarland, P. (2007). Advances in the development of novel cobalt Fischer-Tropsch catalysts for synthesis of long-chain hydrocarbons and clean fuels. Chem. Rev. *107*, 1692–1744.

101. He, Z.H., Jiang, C.S., Wang, K., Wang, Z.Y., Li, N., Wang, W.T., and Liu, Z.T. (2020). Photothermal CO_2 hydrogenation to methanol over a CoO/Co/TiO_2 catalyst in aqueous media under atmospheric pressure. Catal. Today *356*, 579–588.

102. Wang, L., Wang, L., Liu, X., Wang, H., Zhang, W., Yang, Q., Ma, J., Dong, X., Yoo, S.J., Kim, J.-G., et al. (2018). Selective hydrogenation of CO_2 into ethanol over cobalt catalysts. Angew. Chem. Int. Ed. *130*, 6212–6216.

103. Chen, W., Kimpel, T.F., Song, Y., Chiang, F.K., Zijlstra, B., Pestman, R., Wang, P., and Hensen, E.J.M. (2018). Influence of carbon deposits on the cobalt-catalyzed Fischer-Tropsch reaction: evidence of a two-site reaction model. ACS Catal. *8*, 1580–1590.

104. Ono, F., and Maeta, H. (1988). Determination of lattice parameters in Hcp cobalt by using X-ray bond's method. Le J. Phys. Colloq. *49*, C8-63–C8-64.

105. van Helden, P., Ciobîcə, I.M., and Coetzer, R.L.J. (2016). The size-dependent site composition of FCC cobalt nanocrystals. Catal. Today *261*, 48–59.

106. van Helden, P., and Ciobëcă, I.M. (2011). A DFT study of carbon in the subsurface layer of cobalt surfaces. ChemPhysChem *12*, 2925–2928.

107. Kitakami, O., Sato, H., Shimada, Y., Sato, F., and Tanaka, M. (1997). Size effect on the crystal phase of cobalt fine particles. Phys. Rev. B *56*, 849–854.

108. Gnanamani, M.K., Jacobs, G., Keogh, R.A., Shafer, W.D., Sparks, D.E., Hopps, S.D., Thomas, G.A., and Davis, B.H. (2015). Fischer-Tropsch synthesis: effect of pretreatment conditions of cobalt on activity and selectivity for hydrogenation of carbon dioxide. Appl. Catal. A Gen. *499*, 39–46.

109. Liu, J.X., Su, H.Y., Sun, D.P., Zhang, B.Y., and Li, W.X. (2013). Crystallographic dependence of CO activation on cobalt catalysts: HCP versus FCC. J. Am. Chem. Soc. *135*, 16284–16287.

110. Bezemer, G.L., Bitter, J.H., Kuipers, H.P.C.E., Oosterbeek, H., Holewijn, J.E., Xu, X., Kapteijn, F., van Dillen, A.J., and de Jong, K.P. (2006). Cobalt particle size effects in the Fischer-Tropsch reaction studied with carbon nanofiber supported catalysts. J. Am. Chem. Soc. *128*, 3956–3964.

111. Den Breejen, J.P., Radstake, P.B., Bezemer, G.L., Bitter, J.H., Froseth, V., Holmen, A., and de Jong, K.P. (2009). On the origin of the cobalt particle size effects in Fischer-Tropsch catalysis. J. Am. Chem. Soc. *131*, 7197–7203.

112. Foppa, L., Copéret, C., and Comas-Vives, A. (2016). Increased back-bonding explains step-edge reactivity and particle size effect for CO activation on Ru nanoparticles. J. Am. Chem. Soc. *138*, 16655–16668.

113. Iglesia, E. (1997). Design, synthesis, and use of cobalt-based Fischer-Tropsch synthesis catalysts. Appl. Catal. A Gen. *161*, 59–78.

114. Fischer, N., van Steen, E., and Claeys, M. (2011). Preparation of supported nano-sized cobalt oxide and fcc cobalt crystallites. Catal. Today *171*, 174–179.

115. Prieto, G., Martínez, A., Concepción, P., and Moreno-Tost, R. (2009). Cobalt particle size effects in Fischer-Tropsch synthesis: structural and in situ spectroscopic characterisation on reverse micelle-synthesised Co/ITQ-2 model catalysts. J. Catal. *266*, 129–144.

116. Borg, Ø., Dietzel, P.D.C., Spjelkavik, A.I., Tveten, E.Z., Walmsley, J.C., Diplas, S., Eri, S., Holmen, A., and Rytter, E. (2008). Fischer-Tropsch synthesis: cobalt particle size and support effects on intrinsic activity and product distribution. J. Catal. *259*, 161–164.

117. Xiong, H., Motchelaho, M.A.M., Moyo, M., Jewell, L.L., and Coville, N.J. (2011). Correlating the preparation and performance of cobalt catalysts supported on carbon nanotubes and carbon spheres in the Fischer-Tropsch synthesis. J. Catal. *278*, 26–40.

118. Gupta, S., and Carrizosa, S.B. (2015). Graphene–inorganic hybrids with cobalt oxide polymorphs for electrochemical energy systems and electrocatalysis: synthesis, processing and properties. J. Electron. Mater. *44*, 4492–4509.

119. Cats, K.H., Andrews, J.C., Stéphan, O., March, K., Karunakaran, C., Meirer, F., de Groot, F.M.F., and Weckhuysen, B.M. (2016). Active phase distribution changes within a catalyst particle during Fischer–Tropsch synthesis as revealed by multi-scale microscopy. Catal. Sci. Technol. *6*, 4438–4449.

120. Cats, K.H., Gonzalez-Jimenez, I.D., Liu, Y., Nelson, J., van Campen, D., Meirer, F., van der Eerden, A.M.J., de Groot, F.M.F., Andrews, J.C., and Weckhuysen, B.M. (2013). X-ray nanoscopy of cobalt Fischer-Tropsch catalysts at work. Chem. Commun. *49*, 4622–4624.

121. Tsakoumis, N.E., Walmsley, J.C., Rønning, M., van Beek, W., Rytter, E., and Holmen, A. (2017). Evaluation of reoxidation thresholds for γ-Al_2O_3-supported cobalt catalysts under Fischer-Tropsch synthesis conditions. J. Am. Chem. Soc. *139*, 3706–3715.

122. Senecal, P., Jacques, S.D.M., Di Michiel, M., Kimber, S.A.J., Vamvakeros, A., Odarchenko, Y., Lezcano-Gonzalez, I., Paterson, J., Ferguson, E., and Beale, A.M. (2017). Real-time scattering-contrast imaging of a supported cobalt-based catalyst body during activation and Fischer-Tropsch synthesis revealing spatial dependence of particle size and phase on catalytic properties. ACS Catal. *7*, 2284–2293.

123. Wolf, M., Mutuma, B.K., Coville, N.J., Fischer, N., and Claeys, M. (2018). Role of CO in the water-induced formation of cobalt oxide in a high conversion Fischer–Tropsch environment. ACS Catal. *8*, 3985–3989.

124. van Berge, P.J., van de Loosdrecht, J., Barradas, S., and van der Kraan, A.M. (2000). Oxidation of cobalt based Fischer-Tropsch catalysts as a deactivation mechanism. Catal. Today *58*, 321–334.

125. Dubrovin, R.M., Siverin, N.V., Prosnikov, M.A., Chernyshev, V.A., Novikova, N.N., Christianen, P.C.M., Balbashov, A.M., and Pisarev, R.V. (2021). Lattice dynamics and spontaneous magnetodielectric effect in ilmenite $CoTiO_3$. J. Alloys Compd. *858*, 157633.

126. Moodley, D.J., Saib, A.M., van de Loosdrecht, J., Welker-Nieuwoudt, C.A., Sigwebela, B.H., and Niemantsverdriet, J.W. (2011). The impact of cobalt aluminate formation on the deactivation of cobalt-based Fischer-Tropsch synthesis catalysts. Catal. Today *171*, 192–200.

127. Melaet, G., Lindeman, A.E., and Somorjai, G.A. (2014). Cobalt particle size effects in the Fischer-Tropsch synthesis and in the hydrogenation of CO_2 studied with nanoparticle model catalysts on silica. Top. Catal. *57*, 500–507.

128. Nagakura, S. (1961). Study of metallic carbides by electron diffraction Part IV. Cobalt carbides. J. Phys. Soc. Jpn. *16*, 1213–1219.

129. Shein, I.R., Medvedeva, N.I., and Ivanovskii, A.L. (2006). Electronic and structural properties of cementite-type M_3X (M=Fe, Co,

Ni; X=C or B) by first principles calculations. Phys. B Condens. Matter *371*, 126–132.

130. Baker, R.T.K. (1979). In situ electron microscopy studies of catalyst particle behavior. Catal. Rev. Eng. *19*, 161–209.

131. Niemantsverdriet, J.W., and van der Kraan, A.M. (1981). Time-dependent behavior of iron catalysts in Fischer-Tropsch synthesis. J. Catal. *72*, 385–388.

132. Vannice, M.A. (1975). The catalytic synthesis of hydrocarbons from H_2/CO mixtures over the group VIII metals: I. The specific activities and product distributions of supported metals. J. Catal. *37*, 449–461.

133. Wesner, D.A., Linden, G., and Bonzel, H.P. (1986). Alkali promotion on cobalt: surface analysis of the effects of potassium on carbon monoxide adsorption and Fischer-Tropsch reaction. Appl. Surf. Sci. *26*, 335–356.

134. Li, Z., Zhong, L., Yu, F., An, Y., Dai, Y., Yang, Y., Lin, T., Li, S., Wang, H., Gao, P., et al. (2017). Effects of sodium on the catalytic performance of CoMn catalysts for Fischer-Tropsch to olefin reactions. ACS Catal. *7*, 3622–3631.

135. Zhao, Z., Lu, W., Yang, R., Zhu, H., Dong, W., Sun, F., Jiang, Z., Lyu, Y., Liu, T., Du, H., et al. (2018). Insight into the formation of Co@Co_2C catalysts for direct synthesis of higher alcohols and olefins from syngas. ACS Catal. *8*, 228–241.

136. Li, Z., Yu, D., Yang, L., Cen, J., Xiao, K., Yao, N., and Li, X. (2021). Formation mechanism of the Co_2C nanoprisms studied with the CoCe system in the Fischer–Tropsch to olefin reaction. ACS Catal. *11*, 2746–2753.

137. Singh, J.A., Hoffman, A.S., Schumann, J., Boubnov, A., Asundi, A.S., Nathan, S.S., Nørskov, J., Bare, S.R., and Bent, S.F. (2018). Role of Co_2C in ZnO-promoted Co catalysts for alcohol synthesis from syngas. ChemCatChem *11*, 1–11.

138. Zhao, Z., Lu, W., Zhu, H., Dong, W., Lyu, Y., Liu, T., Chen, X., Wang, Y., and Ding, Y. (2018). Tuning the Fischer–Tropsch reaction over Co_xMn_yLa/AC catalysts toward alcohols: effects of La promotion. J. Catal. *361*, 156–167.

139. Wang, X., Chen, W., Lin, T., Li, J., Yu, F., An, Y., Dai, Y., Wang, H., Zhong, L., and Sun, Y. (2018). Effect of the support on cobalt carbide catalysts for sustainable production of olefins from syngas. Chin. J. Catal. *39*, 1869–1880.

140. Athariboroujeny, M., Raub, A., Iablokov, V., Chenakin, S., Kovarik, L., and Kruse, N. (2019). Competing mechanisms in CO hydrogenation over Co-MnO_x catalysts. ACS Catal. *9*, 5603–5612.

141. An, Y., Zhao, Y., Yu, F., Lin, T., Lu, Y., Li, S., Li, Z., Dai, Y., Wang, X., Wang, H., et al. (2018). Morphology control of Co_2C nanostructures via the reduction process for direct production of lower olefins from syngas. J. Catal. *366*, 289–299.

142. Paterson, J., Peacock, M., Purves, R., Partington, R., Sullivan, K., Sunley, G., and Wilson, J. (2018). Manipulation of Fischer-Tropsch synthesis for production of higher alcohols using manganese promoters. ChemCatChem *10*, 5154–5163.

143. Wang, Z., Kumar, N., and Spivey, J.J. (2016). Preparation and characterization of lanthanum-promoted cobalt-copper catalysts for the conversion of syngas to higher oxygenates: formation of cobalt carbide. J. Catal. *339*, 1–8.

144. Han, Y., Fang, C., Ji, X., Wei, J., Ge, Q., and Sun, J. (2020). Interfacing with carbonaceous potassium promoters boosts catalytic CO_2 hydrogenation of iron. ACS Catal. *10*, 12098–12108.

145. Huo, C.-F., Wu, B.-S., Gao, P., Yang, Y., Li, Y.-W., and Jiao, H. (2011). The mechanism of potassium promoter: enhancing the stability of active surfaces. Angew. Chem. Int. Ed. *123*, 7541–7544.

146. Mohandas, J.C., Gnanamani, M.K., Jacobs, G., Ma, W., Ji, Y., Khalid, S., and Davis, B.H. (2011). Fischer-Tropsch synthesis: characterization and reaction testing of cobalt carbide. ACS Catal. *1*, 1581–1588.

147. Dai, Y., Zhao, Y., Lin, T., Li, S., Yu, F., An, Y., Wang, X., Xiao, K., Sun, F., Jiang, Z., et al. (2019). Particle size effects of cobalt carbide for Fischer-Tropsch to olefins. ACS Catal. *9*, 798–809.

148. Liu, B., Li, W., Xu, Y., Lin, Q., Jiang, F., and Liu, X. (2019). Insight into the intrinsic active site for selective production of light olefins in cobalt-catalyzed Fischer-Tropsch synthesis. ACS Catal. *9*, 7073–7089.

149. Xiong, H., Jewell, L.L., and Coville, N.J. (2015). Shaped carbons as supports for the catalytic conversion of syngas to clean fuels. ACS Catal. *5*, 2640–2658.

150. Tauster, S.J., Fung, S.C., and Garten, R.L. (1978). Strong metal-support interactions. Group 8 noble metals supported on TiO_2. J. Am. Chem. Soc. *100*, 170–175.

151. Tauster, S.J., Fung, S.C., Baker, R.T., and Horsley, J.A. (1981). Strong interactions in supported-metal catalysts. Science *211*, 1121–1125.

152. Tauster, S.J. (1987). Strong metal-support interactions. Acc. Chem. Res. *20*, 389–394.

153. Parastaev, A., Muravev, V., Huertas Osta, E., van Hoof, A.J.F., Kimpel, T.F., Kosinov, N., and Hensen, E.J.M. (2020). Boosting CO_2 hydrogenation via size-dependent metal–support interactions in cobalt/ceria-based catalysts. Nat. Catal. *3*, 526–533.

154. Kattel, S., Liu, P., and Chen, J.G. (2017). Tuning selectivity of CO_2 hydrogenation reactions at the metal/oxide interface. J. Am. Chem. Soc. *139*, 9739–9754.

155. Hernández Mejía, C., van Deelen, T.W., and de Jong, K.P. (2018). Activity enhancement of cobalt catalysts by tuning metal-support interactions. Nat. Commun. *9*, 4459.

156. Fu, Q., and Wagner, T. (2007). Interaction of nanostructured metal overlayers with oxide surfaces. Surf. Sci. Rep. *62*, 431–498.

157. Prieto, G., De Mello, M.I.S., Concepción, P., Murciano, R., Pergher, S.B.C., and Martínez, A. (2015). Cobalt-catalyzed Fischer-Tropsch synthesis: chemical nature of the oxide support as a performance descriptor. ACS Catal. *5*, 3323–3335.

158. Boffa, A.B., Lin, C., Bell, A.T., and Somorjai, G.A. (1994). Lewis acidity as an explanation for oxide promotion of metals: implications of its importance and limits for catalytic reactions. Catal. Lett. *27*, 243–249.

159. Vannice, M.A. (1992). Hydrogenation of CO and carbonyl functional groups. Catal. Today *12*, 255–267.

160. Maitlis, P.M., and Zanotti, V. (2009). The role of electrophilic species in the Fischer-Tropsch reaction. Chem. Commun. *13*, 1619–1634.

161. Jiao, G., Ding, Y., Zhu, H., Li, X., Li, J., Lin, R., Dong, W., Gong, L., Pei, Y., and Lu, Y. (2009). Effect of La_2O_3 doping on syntheses of C_1-C_{18} mixed linear α-alcohols from syngas over the Co/AC catalysts. Appl. Catal. A Gen. *36*, 137–142.

162. Xie, J., Paalanen, P.P., van Deelen, T.W., Weckhuysen, B.M., Louwerse, M.J., and de Jong, K.P. (2019). Promoted cobalt metal catalysts suitable for the production of lower olefins from natural gas. Nat. Commun. *10*, 167.

163. Moya-Cancino, J.G., Honkanen, A.P., van der Eerden, A.M.J., Schaink, H., Folkertsma, L., Ghiasi, M., Longo, A., Meirer, F., de Groot, F.M.F., Huotari, S., et al. (2019). Elucidating the K-edge X-ray absorption near-edge structure of cobalt carbide. ChemCatChem *11*, 3042–3045.

164. Moya-Cancino, J.G., Honkanen, A.P., van der Eerden, A.M.J., Schaink, H., Folkertsma, L., Ghiasi, M., Longo, A., de Groot, F.M.F., Meirer, F., Huotari, S., et al. (2019). In-situ X-ray absorption near edge structure spectroscopy of a solid catalyst using a laboratory-based set-up. ChemCatChem *11*, 1039–1044.

165. van Ravenhorst, I.K., Ho, A.S., Vogt, C., Boubnov, A., Patra, N., Oord, R., Akatay, C., Meirer, F., Bare, S.R., and Weckhuysen, B.M. (2021). On the cobalt carbide formation in a Co/TiO_2 Fischer–Tropsch synthesis catalyst as studied by high-pressure, long-term operando X-ray absorption and diffraction. ACS Catal. *11*, 2956–2967.

166. Balachandran, U., and Eror, N.G. (1982). Raman spectra of titanium dioxide. J. Solid State Chem. *42*, 276–282.

167. Cromer, D.T., and Herrington, K. (1955). The structures of anatase and rutile. J. Am. Chem. Soc. *77*, 4708–4709.

168. Hitchcock, A.P. (2015). Soft X-ray spectromicroscopy and ptychography. J. Electron Spectros. Relat. Phenomena *200*, 49–63.

169. Andrews, J.C., and Weckhuysen, B.M. (2013). Hard X-ray spectroscopic nano-imaging of hierarchical functional materials at work. ChemPhysChem *14*, 3655–3666.

170. dapted from: http://henke.lbl.gov/optical_constants/atten2.html.

171. Xiong, L. Bin, Li, J.L., Yang, B., and Yu, Y. (2012). Ti^{3+} in the surface of titanium dioxide: generation, properties and

photocatalytic application. J. Nanomater. *2012*, 831524.

172. Nowak, D., Morrison, W., Wickramasinghe, H.K., Jahng, J., Potma, E., Wan, L., Ruiz, R., Albrecht, T.R., Schmidt, K., Frommer, J., et al. (2016). Nanoscale chemical imaging by photoinduced force microscopy. Sci. Adv. *2*, e1501571.

173. Bechtel, H.A., Johnson, S.C., Khatib, O., Muller, E.A., and Raschke, M.B. (2020). Synchrotron infrared nano-spectroscopy and -imaging. Surf. Sci. Rep. *75*, 100493.

174. Hartman, T., Wondergem, C.S., Kumar, N., van den Berg, A., and Weckhuysen, B.M. (2016). Surface- and tip-enhanced Raman spectroscopy in catalysis. J. Phys. Chem. Lett. *7*, 1570–1584.

175. van Schrojenstein Lantman, E.M., Deckert-Gaudig, T., Mank, A.J.G., Deckert, V., and Weckhuysen, B.M. (2012). Catalytic processes monitored at the nanoscale with tip-enhanced Raman spectroscopy. Nat. Nanotechnol. *7*, 583–586.

176. Fu, D., Park, K., Delen, G., Attila, Ö., Meirer, F., Nowak, D., Park, S., Schmidt, J.E., and Weckhuysen, B.M. (2017). Nanoscale infrared imaging of zeolites using photoinduced force microscopy. Chem. Commun. *53*, 18–21.

177. Wu, C.Y., Wolf, W.J., Levartovsky, Y., Bechtel, H.A., Martin, M.C., Toste, F.D., and Gross, E. (2017). High-spatial-resolution mapping of catalytic reactions on single particles. Nature *541*, 511–515.

178. Zhong, L., Chen, D., and Zafeiratos, S. (2019). A mini review of in situ near-ambient pressure XPS studies on non-noble, late transition metal catalysts. Catal. Sci. Technol. *9*, 3851–3867.

179. De Smit, E., Cinquini, F., Beale, A.M., Safonova, O.V., van Beek, W., Sautet, P., and Weckhuysen, B.M. (2010). Stability and reactivity of ε-X-θ iron carbide catalyst phases in Fischer-Tropsch synthesis: controlling μc. J. Am. Chem. Soc. *132*, 14928–14941.

180. Last, G.V., and Schmick, M.T. (2015). A review of major non-power-related carbon dioxide stream compositions. Environ. Earth Sci. *74*, 1189–1198.

181. Tsakoumis, N.E., Dehghan, R., Johnsen, R.E., Voronov, A., van Beek, W., Walmsley, J.C., Borg, Ø., Rytter, E., Chen, D., Rønning, M., et al. (2013). A combined in situ XAS-XRPD-Raman study of Fischer-Tropsch synthesis over a carbon supported Co catalyst. Catal. Today *205*, 86–93.

182. van der Laan, G.P., and Beenackers, A.A.C.M. (1999). Kinetics and selectivity of the Fischer-Tropsch synthesis: a literature review. Catal. Rev. Sci. Eng. *41*, 255–318.

183. Liu, Y., Wu, D., Yu, F., Yang, R., Zhang, H., Sun, F., Zhong, L., and Jiang, Z. (2019). In situ XAFS study on the formation process of cobalt carbide by Fischer-Tropsch reaction. Phys. Chem. Chem. Phys. *21*, 10791–10797.